U.S. DEPARTMENT OF COMMERCE
National Technical Information Service

PB-280 126

Development and Fabrication of a Prototype Fibrous Aerosol Monitor (FAM)

GCA Corp, Bedford, Mass GCA Technology Div

Prepared for

National Inst for Occupational Safety and Health, Cincinnati, Ohio Div of Physical Sciences and Engineering

Dec 77

HEW	United States Department of Health, Education, and Welfare	Public Health Service, Center for Disease Control National Institute for Occupational Safety and Health Cincinnati, Ohio 45226	DHEW(NIOSH)Pub.. No. 78-125
EPA	United States Environmental Protection Agency	Office of Energy, Minerals, and Industry Office of Research and Development Washington, D.C. 20460	EPA-600/7-77-147 December 1977

PB 280 126

DEVELOPMENT AND FABRICATION OF A PROTOTYPE FIBROUS AEROSOL MONITOR (FAM)

Interagency
Energy-Environment
Research and Development
Program Report

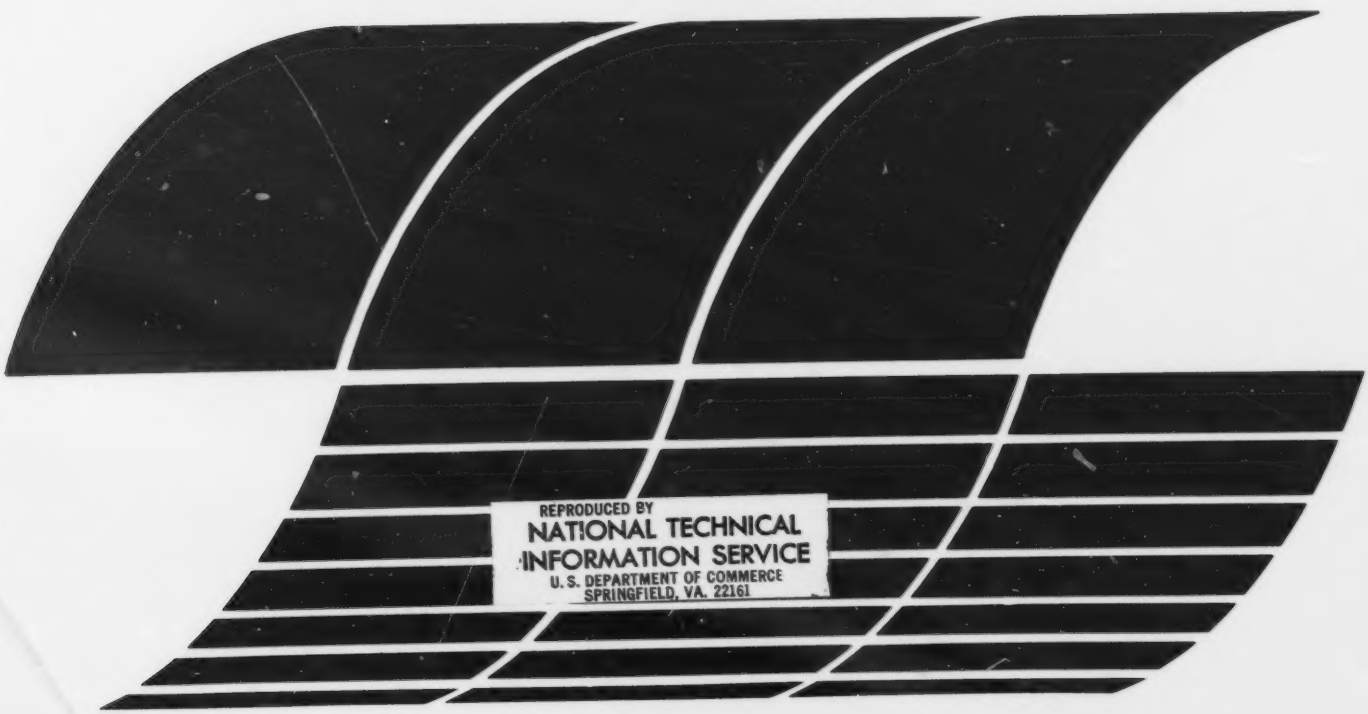

REPRODUCED BY
NATIONAL TECHNICAL
INFORMATION SERVICE
U.S. DEPARTMENT OF COMMERCE
SPRINGFIELD, VA. 22161

TECHNICAL REPORT DATA
(Please read Instructions on the reverse before completing)

1. REPORT NO. EPA-600/7-77-147	2.
3. RECIPIENT'S ACCESSION NO. PB280126	
TITLE AND SUBTITLE: Development and Fabrication of a Prototype Fibrous Aerosol Monitor (FAM)	5. REPORT DATE: December 1977 issuing date
	6. PERFORMING ORGANIZATION CODE
7. AUTHOR(S): Pedro Lilienfeld and Paul B. Elterman	8. PERFORMING ORGANIZATION REPORT NO.
9. PERFORMING ORGANIZATION NAME AND ADDRESS: NIOSH, Cincinnati, Ohio 45226/IAG; GCA/Technology Division, Bedford, Massachusetts 01730	10. PROGRAM ELEMENT NO. INE-625
	11. CONTRACT/GRANT NO. IAG-D7-E773-DE-BDE
12. SPONSORING AGENCY NAME AND ADDRESS: Office of Energy, Minerals, & Industry; Office of Research & Development; U.S. Environmental Protection Agency; Washington, D.C. 20460	13. TYPE OF REPORT AND PERIOD COVERED: Milestone
	14. SPONSORING AGENCY CODE: EPA/600/17

15. SUPPLEMENTARY NOTES
This project is part of the EPA-planned and coordinated Federal Interagency Energy/Environment R&D Program. (P.O.: G.J. D'Alessio, 8-426-4568) Headquarters

16. ABSTRACT

This report describes a program whose objective was to develop, design, fabricate and laboratory-test two prototype instruments capable of real-time selective detection and measurement of airborne fibrous-shaped particles. The selective detection of the fibers is effected by synchronous detection of the resulting modulation of the light scattered from a continuous-wave helium-neon laser beam by the rotating particles. The theory of operation, design of the electric-optical detection configuration and the electronic signal processing method are discussed. By means of a scattering pulse sharpness discrimination technique, fibers whose length exceed a selectable value are detected and their number concentration digitally displayed. A concentration of the order of one fiber per cubic centimeter can be assessed within a relative standard deviation of 10 percent with a counting period of 10 minutes. The FAM is a portable, battery-powered instrument capable of operating continuously for about 4 hours between battery charges. Preliminary tests with crocidolite and crysotile asbestos as well as with glass fibers were performed in the laboratory and the results indicate good correlation with the standard NIOSH phase contrast microscopy filter counting method.

17. (Circle One or More) KEY WORDS AND DOCUMENT ANALYSIS

a. DESCRIPTORS	b. IDENTIFIERS/OPEN ENDED TERMS	c. COSATI Field/Group
Ecology Environments Earth Atmosphere Environmental Engineering	[illegible]	6F 97G

18. DISTRIBUTION STATEMENT: Release to Public	19. SECURITY CLASS (This Report): Unclassified	21. NO. OF PAGES: 86
	20. SECURITY CLASS (This page): Unclassified	22. PRICE: PC A05 MF A01

DEVELOPMENT AND FABRICATION OF A PROTOTYPE FIBROUS AEROSOL MONITOR (FAM)

Pedro Lilienfeld
Paul B. Elterman

GCA CORPORATION
GCA/TECHNOLOGY DIVISION
Bedford, Massachusetts

Contract No. 210-76-0110

U.S. DEPARTMENT OF HEALTH, EDUCATION, AND WELFARE
Public Health Service
National Institute for Occupational Safety and Health
Division of Physical Sciences and Engineering
Cincinnati, Ohio 45226

December 1977

DISCLAIMER

The contents of this report are reproduced herein as received from the contractor.

The opinions, findings, and conclusions expressed herein are not necessarily those of the National Institute for Occupational Safety and Health, nor does mention of company names or products constitute endorsement by the National Institute for Occupational Safety and Health.

NIOSH Project Officer: Paul Baron
Principal Investigator: Pedro Lilienfeld

Partial funding of this project was provided by the Environmental Protection Agency under the Energy/Environmental R and D Program.

DHEW (NIOSH) Publication No. 78-125

ABSTRACT

This report describes a program whose objective was to develop, design, fabricate and laboratory-test two prototype instruments capable of real-time selective detection and measurement of airborne fibrous-shaped particles.

The operation of this fibrous aerosol monitor (FAM) is based on the rotation imparted to the acicular particles by means of a rotating quadrupole electric field of the order of 3000 V/cm. This field induces a dipole charge separation on the fibers and aligns them with the applied field. The selective detection of the fibers is effected by synchronous detection of the resulting modulation of the light scattered from a continuous-wave helium-neon laser beam by the rotating particles.

The theory of operation, design of the electric-optical detection configuration and the electronic signal processing method are discussed. By means of a scattering pulse sharpness discrimination technique, fibers whose length exceed a selectable value are detected and their number concentration digitally displayed. Counting times of 1 to 1000 minutes permit the measurement of fiber concentrations between 0.001 and about 30 cm^{-3}. A concentration of the order of one fiber per cubic centimeter can be assessed within a relative standard deviation of 10 percent with a counting period of 10 minutes.

The FAM is a portable, battery-powered instrument capable of operating continuously for about 4 hours between battery charges. Preliminary tests with crocidolite and crysotile asbestos as well as with glass fibers were performed in the laboratory and the results indicate good correlation with the standard NIOSH phase contrast microscopy filter counting method.

CONTENTS

Abstract iii
Acknowledgments viii
Introduction 1
Theory 3
    Principle of Operation 3
    Electric Field-Induced Fiber Alignment 4
    Light Scattering by Fibrous-Shaped Particles 11
    Single Fiber Detection Statistics and Flow Considerations 20
    Rectilinear Aerodynamic Behavior of Airborne Fibers 22
Prototype Instrument Development 27
    Laboratory Test System 27
    Prototype Design 33
    Prototype Aerosol Testing 49
Prototype Instrument Instruction Manual 55
    Specifications 55
    Operating Procedures 56
    Electronic Testing and Adjustment Procedures 59
    Optical Alignment Procedure and Cleaning 61
    Safety Aspects 63
References 64
Conclusions and Recommendations 67
Appendix A 69

Preceding page blank

FIGURES

1. Phase lag between the fiber axis and rotating electric field vector as a function of fiber length-to-diameter ratio and field intensity for $\omega = 2\pi \cdot 400\ sec^{-1}$, $\eta = 1.8 \times 10^{-4}$ poise, and $\varepsilon = 5$. 8
2. Quadrupole field configuration 10
3. Light scattering-electric field geometry 12
4. Pulse shape as a function of fiber length 14
5. Detection pulse shape for a 4 μm long fiber ($\lambda = 0.6328$ μm) and gating intervals for the ratio method of fiber length determination 17
6. Detection pulse shape for a 6 μm long fiber ($\lambda = 0.6328$ μm) and gating intervals for the ratio method of fiber length determination 18
7. Ratio signal as a function of fiber length 19
8. Sedimentation of ellipsoids, i) axis parallel to direction of motion; ii) axis normal to direction of motion 25
9. Schematic of initial version of the circuitry used to generate rotating electric field 28
10. Flow test system used to observe air flow streamlines 30
11. Hydrolized bed aerosol generator 34
12. Schematic of optical and flow systems of FAM 35
13. Optical and flow elements of the FAM 36
14. FAM quadrature field gen and driver board 40
15. FAM overall wiring layout 41
16. Overall block diagram of electronic subsystem of the FAM 43
17. FAM gating and processing board 44
18. FAM counter and display boards 46
19. Battery output voltage as a function of FAM operating time 48
20. View of bottom of FAM enclosure with panel removed 50
21. Top view of FAM with electronic circuitry card cage in the lifted-up position 51
22. FAM test data 53
23. Top view of FAM 57
24. Top views of quadrature field generator-driver and of gating-processing boards 60
25. Top view of counter-display board 62

TABLES

1. Comparison of fiber lengths as a function of nebulizer operation generation time 32
2. Comparison of fiber lengths as a function of nebulizer operation time 32
3. Test data of FAM 54

ACKNOWLEDGMENTS

We wish to acknowledge the crucial contributions to the execution of this development program of M. Yagjian, D. Anderson, R. Stern, and A. Armstrong of the GCA/Technology Division, as well as the seminal participation of Dr. D. Cooper of Harvard University.

INTRODUCTION

The presence of fibrous-shaped airborne particles, in particular asbestos dust, has been found to result in several serious human respiratory ailments among which asbestosis and lung cancer are salient, [1,2,3] In addition, fibers of other substances such as glass, talc and textiles are suspected of being causatory agents in similar pulmonary problems. The commonality of the use of asbestos as a construction and insulation material has resulted in its pervasive presence and in frequently unsuspected contamination of both enclosed spaces as well as open air environments.

The pathological effects of such dusts have been found to be correlated and directly associated with the retention of fibrous-shaped particles with lengths typically exceeding about 5 μm.

The high correlation of cause and effect between the exposure of asbestos industry workers to these fibers and their respiratory pathology has resulted in stringent regulations[4] in terms of 8-hour shift exposure concentrations of asbestos fibers, and a continuous trend in reducing the threshold limit values for such concentrations has been pursued and will probably continue in the foreseable future.

The detection and measurement of the concentration of airborne fibers is obviously a crucial requirement in any industrial protection program, in the assessment of potential dangers, and for the enforcement of regulations. The only method, presently accepted, for the determination of the concentration of airborne fibers; e.g. asbestos in its various forms, consists of manual counting and sizing of such fibers by phase-contrast microscopy of samples collected by filtration on membrane media.[5-8] This method is relatively imprecise since it is subjected to human interpretation and concomitant errors. In addition, the process involves significant and in many cases intolerable time delays before the information becomes available and can be fed back for the implementation of corrective and/or protective measures. Although integrated shift exposure will, at least for the time being, rely on the above-mentioned method of assessment, an urgent requirement exists for an instrument capable of providing real-time measurements of the concentration of airborne particles of fibrous (or acicular) shape. No such monitoring device, compatible with field use, portability, and the capability to size-selectively count fibers has been available to date, although several conceptually feasible solutions have been and continue to be explored.[9,10]

Within this background, the GCA/Technology Division endeavored to develop a practical, field-worthy instrument for the on-the-spot selective detection, counting and sizing of discrete acicular-shaped particles, even in the presence of nonfibrous particle concentrations several orders of magnitude higher than those of the particles of interest. The present report describes the development program pursued under a NIOSH contract whose objective was to develop and fabricate two identical prototype instruments to detect exclusively fibrous aerosols and to measure the number concentrations of fibers in the range of 0.1 to 20 cm^{-3}, with diameters exceeding 0.1 μm and lengths exceeding 5 μm.

Further requirements and specification objectives were: relative standard deviation of a measurement within 10 percent for a constant concentration of five fibers/cm^3 and a measurement time of 3 minutes or less; battery and/or line operation with a battery supply compatible with a 4-hour continuous operation without external power input; maximum weight and overall volume of 13.6 kg and 0.057 m^3, respectively.

The program included a theoretical effort whose objectives were to relate the physical dimensions of the fibers to the parameters sensed by the instrument, and to characterize and optimize the operational parameters of the system.

The principle on which the Fibrous Aerosol Monitor (henceforth called FAM) is based is a result of the combination of electrostatic and light scattering properties of fibrous-shaped particles. A continuously flowing sample stream of air is subjected to a high intensity rotating electric field and concurrent illumination by a parallel beam of monochromatic light from a continuous wave gas laser. Fibers present in the sample stream are aligned by dipole charge separation with the electric field whose lines of force are perpendicular to the illuminating light beam. The ensuing fiber rotation is synchronous with the applied field and results in a pulsed modulation of the light scattered within the plane of fiber rotation. Individual fibers are thus detected in the form of pulse train bursts whose frequency and phase (with respect to the driving field frequency) are known. Phase sensitive electronic amplification is used in order to improve the signal-to-noise ratio in the presence of noise associated with nonfibrous-shaped particles and other sources of spurious light reaching the detector.

The theoretical work was pursued concurrently with the optical, electronic and mechanical design effort whose objective was the development and fabrication of two field-worthy prototype instruments. Laboratory testing of the electro-optical system played an important role in the experimental facets of this development. Among the peripheral, although vitally important, efforts of this program was the design and development o a reliable fiber aerosol generator without which the success of this intensive instrument development program would have been rather questionable.

THEORY

PRINCIPLE OF OPERATION

The FAM bases its operation on a two-step sensing procedure: (a) inducing the fibers to rotate rapidly by the application of a rotating high-intensity electric field, and (b) detecting the light scattering signature associated with these fibers as they are illuminated by a monochromatic light beam.

Because the frequency of the light scattering pulses thus produced is known, synchronous or lock-in electronic signal detection can be used in order to greatly enhance the signal-to-noise ratio. Each individual fiber detected in this manner generates a pulse train as it rotates describing a helical trajectory resulting from the combined effects of the rectilinear air flow and the perpendicular field-induced rotation. Fiber length discrimination is achieved by sensing pulse sharpness, since longer fibers produce narrower pulses than shorter ones. The detailed description and the theory underlying this length discrimination method will be presented further ahead in this report.

The technique of induced fiber rotation and concurrent detection of the resulting light scattering signature results in a powerful discriminatory method for the selective counting of airborne fibers even in the concomitant presence of other, nonacicular, particles in concentrations exceeding those of fibers by factors of up to 10^6.

The overall technique required the combination and solution, for the first time within a practical instrument concept, of such phenomena as electrostatic polarizability, field-induced rotation against Stokes-type air viscosity forces and randomization by Brownian bombardment, within a laminar fully-developed parabolic flow profile regime, detection of 90° light scattering pulse trains and the characterization and discrimination of the pulse shape of these fiber-associated trains.

The general idea of electric field-induced alignment of elongated particles such as long molecular chains, rod-like crystals, filamentous viruses, etc., in liquid suspensions, and characterizing their properties by observing the bulk light-scattering behavior of the suspension has been applied and studied during the last 40 years.[11-17] Particle polarizability, light scattering properties, rotational diffusion constants, determination of the diameter distributions of rod-like particles, and in general characterization of such particles in liquid suspensions have been objectives of such investigations. The experimental approach used in the majority of these studies consisted of exposing a sample of the colloidal suspension under scrutiny to a bipolar electric field; i.e., two parallel plates with either a d.c. or an a.c. applied potential. Sample illumination by an incandescent source and bulk light scattering detection by means of photomultipliers were typical. Polarization and relaxation properties

have thus been investigated using the sudden application and interruption of d.c. fields, whereas the use of a.c. fields has been applied to similar objectives as well as to more detailed characterizations made possible by the use of sophisticated techniques such as synchronous detection of the light scattering signal.

Within this background, the idea of applying the fiber alignment-light scattering sensing approach to the selective detection of airborne fibers was developed at the GCA/Technology Division. Initially, as stimulated by the above cited liquid suspension studies, the objective of detecting bulk light scattering oscillations produced by the application to a volume of air of an alternating field between two electrodes was considered. This approach was used, indeed, to initially (i.e., prior to this instrument development program) establish the feasibility of the overall method, but questions arose as to the ability of this approach to provide useful quantitative information on fiber number concentration and size. The two-electrodes a.c. approach produces fiber alignment when the field maxima occur, and relies on randomization of fiber orientation as the field intensity passes through zero; this results in a fiber motion whose amplitude is an inverse function of the field frequency; i.e., shorter time between field maxima reduces the deviation associated with fiber randomization due to Brownian bombardment. It was decided that a more controlled fiber rotation, that could be extended to higher frequencies, could be achieved by the use of a rotating electric field within which the fibers would be under the continuous influence of a field of constant intensity.

The requirement for discrete fiber detection, as opposed to the mere detection of the presence of fibers, imposed far more stringent demands on the method of optical sensing and electronic signal processing, as well as on the flow regime and dimensional constraints of the system.

The subsequent sections will present a somewhat more detailed treatment of the various central aspects of this technique. The scope of this presentation, however, will be limited to the essentials involved with specific emphasis on the aspects most specific to this instrument design.

ELECTRIC FIELD-INDUCED FIBER ALIGNMENT

Fiber Orientation and Rotational Dynamics

The orientation or alignment of fibers; i.e., elongated or acicular particles, suspended in a gaseous or liquid matrix can be accomplished by several means; e.g., by the application of electric fields, magnetic fields or by flow-shear forces. Although magnetic fields have been used for the orientation of certain types of asbestos fibers,[18,19] the use of an electric field presented a number of advantages within the present development, such as: more universal applicability to all types of fibers, without restrictions imposed by their magnetic properties, and greater simplicity and reduced power and weight requirements for the generation of relatively intense fields. Flow-shear alignment is limited to fiber axis orientations parallel to the direction of flow under laminar conditions, and is thus not applicable to the generation of more complex motions such as fiber rotation.

Fiber alignment with an applied electric field implies the generation of a torque resulting from the interaction of the external field and the field-induced dipole moment. This moment is associated with the electric polarization of the elongated particle. In dielectric (i.e., nonconducting) materials, polarization is associated principally with electronic and atomic charge distortion and orientation. Conductive materials or semiconductors exhibit polarization mainly due to field-induced charge migration also called space charge polarization. This latter mechanism probably plays a predominant role in the creation of the dipole moment and the resulting torque in an applied electric field for fibrous-shaped aerosol particles. The observed behavior of fibers subjected to a rotational electric field, during the experimental phase of this program was consistent with the assumption that these particles are electrically conductive. This observation confirms Fuchs'[20] contention that ..." in practice, aerosol particles can be considered conducting...," although preliminary empirical evidence gathered during the closing phases of this program indicates that this assumption may not apply to all types of fibrous particles under all environmental conditions (see section on Prototype Testing).

The degree to which an acicular particle can be aligned with an applied electric field, in the absence of turbulence, depends on the opposing effects of the orienting force; i.e., the interaction of the field and the dipole moment, and the randomizing forces resulting from Brownian molecular bombardment. The torque resulting from shear flow associated with laminar regimes will be neglected in this treatment mainly because within the configuration under scrutiny the fibers are sensed very near to the flow axis where the radial flow velocity gradient is negligible.

The basic equation of motion governing the rotation of elongated particles is given by:[20]

$$d\theta/dt = B_\omega \tau_\theta = \omega \qquad (1)$$

where θ is angular measure of orientation

B_ω is angular or rotation mobility

τ_θ is the torque = $d\Omega/d\theta$, and

Ω is the change in field energy caused by particle polarization.

The general equation of the angular mobility for a prolate ellipsoid is:*

$$B_\omega = \frac{3\left[\frac{2\beta^2 - 1}{\sqrt{\beta^2 - 1}} \ln\left(\beta + \sqrt{\beta^2 - 1}\right) - \beta\right]}{16\pi\eta a^3(\beta^4 - 1)} \qquad (2)$$

* For reasons of simplicity and consistency with Fuchs' treatment[20] these equations are based on the c.g.s. and electrostatic system of units.

where η is the coefficient of viscosity of the gas

a is fiber radius (d/2), and

β is length to diameter ratio of the particle (L/d).

For large values of β (i.e., $\beta > 10$) equation (2) can be replaced by:

$$B_\omega = \frac{3(2\ell n(2\beta) - 1)}{2\pi\eta L^3} \tag{3}$$

For conducting fibers the mean torque on the elongated particle is obtained by differentiation of the expression:

$$\Omega = -\frac{VE^2}{2}\left(\frac{\cos^2\theta}{\chi_1} + \frac{\sin^2\theta}{\chi_2}\right) \tag{4}$$

where V is particle volume,

E is the electric field intensity, and

χ_1 and χ_2 are defined as:

$$\chi_1 = \frac{1}{\beta^2 - 1}\left[\frac{\beta}{\sqrt{\beta^2 - 1}}\,\ell n\left(\beta + \sqrt{\beta^2 - 1}\right) - 1\right] \tag{5}$$

$$\chi_2 = \frac{\beta}{2(\beta^2 - 1)}\left[\beta - \frac{1}{\sqrt{\beta^2 - 1}}\,\ell n\,(\beta + \sqrt{\beta^2 - 1})\right] \tag{6}$$

Thus the torque is equal to:

$$\tau = VE^2 \cos\theta \sin\theta\left(\frac{1}{\chi_1} - \frac{1}{\chi_2}\right) \tag{7}$$

From equations (1), (3) and (7) we obtain:

$$\omega = \frac{3\ (2\ \ell n(2\beta) - 1)}{2\pi\eta L^3}\ \frac{VE^2}{2}\ \sin 2\theta\left(\frac{1}{\chi_1} - \frac{1}{\chi_2}\right) \tag{8}$$

which for large values of β, and since $V = \frac{\pi d^2}{4} L$, can be reduced to:

$$\omega = \frac{3E^2}{16\eta}\ \frac{(2\ \ell n\ (2\beta) - 1)}{(\ell n\ (2\beta) - 1)}\ \sin 2\theta \tag{9}$$

From equation (9) we can write the expression for the phase angle θ between the electric field vector and the axis of the prolate ellipsoid (i.e., the fiber axis):

$$\sin 2\theta = \frac{16\eta\omega\,(\ell n\, 2\beta - 1)}{3\,E^2(2\,\ell n\, 2\beta - 1)} \tag{10}$$

Since the maximum torque occurs at $\theta = 45^{o}$, if the phase lag between the fiber axis and the field vector exceeds that angle the particle can no longer follow the field rotation and its rotation falls out of synchronism with the applied field frequency.

If the same assumption is made as for the above case; i.e., $\beta > 10$, the corresponding equation for dielectric fibers, whose dielectric constant is ε is:

$$\sin 2\theta = \frac{32\eta\omega\beta^2}{3E^2}\,\frac{\varepsilon + 1}{(2\,\ell n\, 2\beta - 1)(\varepsilon - 1)^2} \tag{11}$$

Equations (10) and (11) are plotted on Figure 1 for $\omega = 2\pi \times 400\ \text{sec}^{-1}$ which was the frequency selected for the final prototype version. A discussion of the rationale underlying the selection of that particular field frequency will be presented in a subsequent section of this report. Equation (11) was plotted using $\varepsilon = 5$ (typical for asbestos). Upon inspection of the curves depicted on Figure 1 it becomes apparent that the behavior of conductive and that of nonconductive fibers is very different with respect to the dependence of phase angle on the length-to-diameter ratio of the fibers. Conductive acicular particles rotate with a phase angle essentially independent of the value of L/d, whereas this angle is strongly dependent on that ratio for nonconductive fibers. In addition, dielectric fibers are far more difficult to align with the field than conductive ones; e.g., for a field intensity of 5000 V/cm (16.67 stat volts/cm for equations (10) and (11)) and for an L/d of 20 the phase angle is more than 100 times larger for the nonconductive particles than for the conductive case. Similarly, for a field of about 3000 V/cm (10 stat volts/cm) fibers with an L/d exceeding about 19 cannot be aligned unless they are conductive. The relevant experimental observations that indicate that the behavior of the fibers appears to be more closely approximated by the conductive model will be presented further ahead. In this context it should be considered that small fiber resistivities many decades higher than those commonly accepted as typical of conductors still result in predominantly conductive behavior at frequencies of the order of 400 hertz. In fact, because of the exceedingly small capacitance of a fiber having the typical dimensions of the order of 1 μm diameter and 10 μm length ($\sim 10^{-19}$ farads), resistivities as high as of the order of 10^{13} ohms/square result in charge transport time constants of the order of 10^{-5} sec; i.e., considerably shorter than the period of the 400 Hz field frequency. Some questions remain, however, whether a clearly defined classification of many fibers into either conductive or dielectric is possible, and the existence of transitional and nonohmic (nonlinear resistivity) conditions may have to be considered for a more rigorous characterization of the behavior of asbestos, glass and other types of fibers.

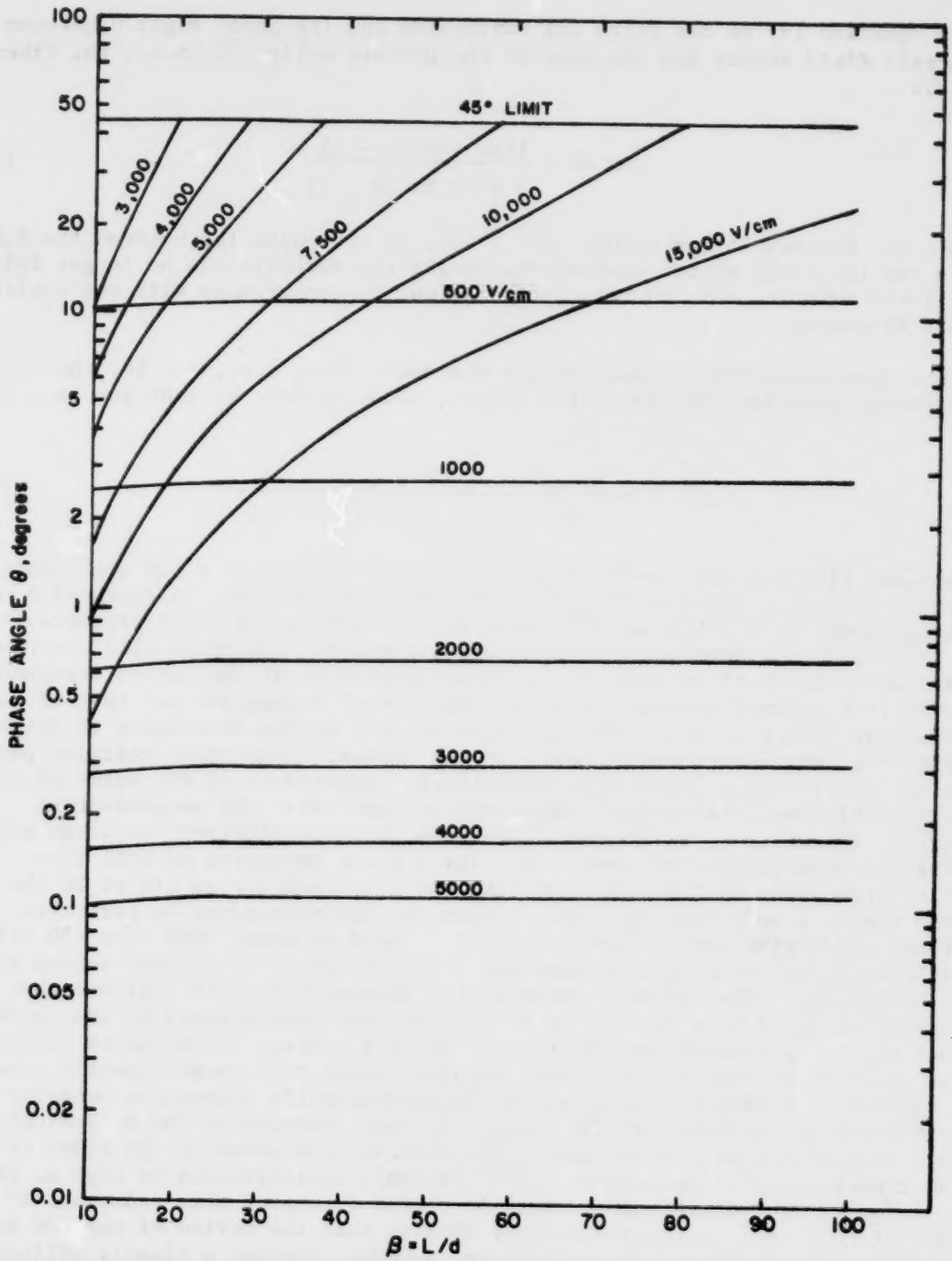

Figure 1. Phase lag between the fiber axis and rotating electric field vector as a function of fiber length-to-diameter ratio and field intensity for $\omega = 2\pi \cdot 400$ sec^{-1}, $\eta = 1.8 \times 10^{-4}$ poise, and $\varepsilon = 5$ (equations 10 and 11). Nearly horizontal curves are for conductive fibers, curves in upper left are for dielectric fibers.

Quadrupole Rotational Electric Field

In order to impart a continuously rotating component to the fiber motion as it passes through the detection region of the FAM a quadrupole field configuration was selected. The electrodes consist of four equally-spaced sectors with cylindrical symmetry. For flow-dynamic reasons (i.e., in order to prevent localized turbulence and eddy formation) these electrodes were designed in the form of conductive foils attached to the inner surface of a glass cylinder. In theory these electrodes could be exterior to the insulating support cylinder, however, this latter solution was found to be electrically unstable because of its sensitivity to any contamination of the inner dielectric surface. The rigorous mathematical characterization of the electric field intensity distribution throughout the volume enclosed by the quadrupole both as a function of radial distance and time, requires a rather complicated treatment which is beyond the scope of this work.

An approximate solution to the field intensity at the axis of quadrupole; i.e., the region of interest in this case, can be obtained by taking only the first term of the series expansion:[21]

$$V(r,\theta) = \sum_{n=1}^{\infty} \frac{1}{\pi \eta a^n} (C_n \cos \eta\theta + D_n \sin \eta\theta) r^n \qquad (12)$$

where $C_n \equiv 2(V_1 + V_2) \sin \frac{\eta\pi}{2}$ and $D_n \equiv (V_1 - V_2)(1 - \cos \eta\pi)$

and V_1 and V_2 are the peak amplitudes with respect to ground of the potentials between the two pairs of opposing electrodes; i.e., one-half of the peak amplitude of the applied potentials, a is the radius of the electrodes and r is the radial distance. Figure 2 illustrates these parameters and the quadrupole configuration. Of the series expressed by equation (12) only the first term contributes significantly to the field near the axis of the system, the second term becomes zero and the third is already of negligible magnitude compared with the first one and since in this case $V_1 = V_2 = V$, the approximate expression for the axial field becomes:

$$E_1 = \frac{4}{\pi} \frac{V}{a} \qquad (13)$$

The coefficient $4/\pi$ represents the electric field enhancement at the axis of the quadrupole due to the focusing effect of the concave shape of the field electrodes; i.e., the field at the axis is $4/\pi$ times higher than that resulting from a uniform field (parallel electrode configuration). This focusing field may tend to contribute to the stability of the axial motion of fibers passing through the sensing volume.

Equation (13) is a reasonably good approximation of the field magnitude at the system sensing volume both for the axis of the quadrupole as well as a function of time (or θ) assuming sinusoidally varying applied potentials.

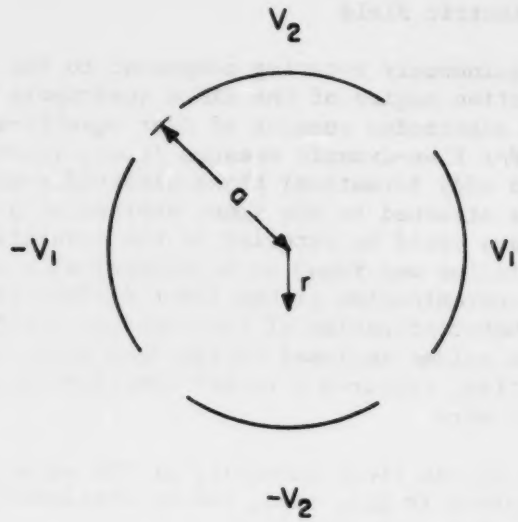

Figure 2. Quadrupole field configuration

LIGHT SCATTERING BY FIBROUS-SHAPED PARTICLES

General Discussion

Light scattering equations in the Mie region; i.e., when the dimensions of the scatterer are of the same order as those of the illuminating wavelength, are notoriously complex even for spheres. The only other particle shape that has been treated extensively in the literature from the point of view of scattering properties are cylinders,[22-27] whose scattering functions are even more complicated than those of spheres as two additional angular dependences must be included; i.e., the angle between the direction of illumination and the cylinder axis and the angle between this axis and the direction of observation. This problem becomes more tractable, however, for specific limiting cases. For the present configuration, the axis of the scattering cylinder rotates in a plane normal to the direction of the illuminating beam; i.e., the case of perpendicular incidence of light on the cylinder axis which is equivalent to a constant, maximum illumination on the scatterer.[28] A further simplification results from the choice of a scattering angle of observation of 90^{o} from the forward direction; i.e., the detector axis lies in the plane of cylinder rotation.

The primary assumption being made with respect to fiber shape is that it can be approximated by a cylinder. The scattering analysis of irregularly-shaped fibers is totally intractable and their detection can only be approached in a totally empirical manner as will be discussed further on within this document. On the other hand it must be considered that several types of fibrous aerosol particles, such as amosite and crocidolite asbestos, and glass fibers are in most cases straight cylinders whose light scattering behavior is well modeled by the cylindrical assumption.

90° Scattering of Cylinders With Perpendicular Illumination

The choice of the 90° scattering angle was based on simplicity of instrument design and signal processing. For this angle the modulation of the scattered light is nearly 100 percent because the projected fiber area viewed by the detector undergoes the largest excursion during each semirotation. This can best be understood when considering the other two limiting scattering angles of 0° and 180° where the modulation due to the fiber rotation goes to zero; i.e., the fiber axis would always be viewed perpendicularly and no fiber-selective signal would be detected.

Figure 3 depicts the essential geometrical configuration of the relevant scattering and illuminating angles, and the relative position of the orienting quadrupole field electrodes.

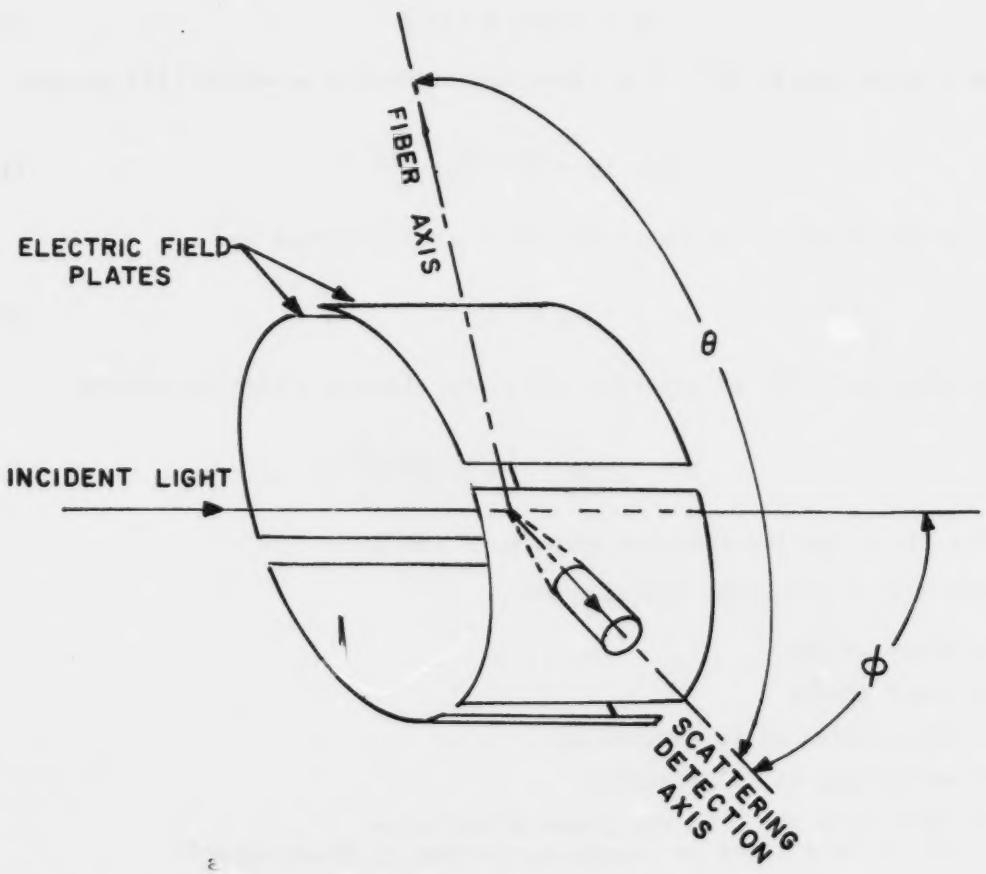

Figure 3. Light scattering-electric field geometry

The fibers scatter a maximum in the direction perpendicular to their axis, thus for every complete fiber rotation two light scattering maxima or peaks are detected within the configuration of Figure 3. This angular dependence of the light scattered by a cylinder can be compared with a rotating search-light beam, or with the emission of a pulsar, in that the detected signal is very sharply peaked at the maxima and nearly zero at all other angles (or times, for a uniformly rotating fiber). In fact, it is the degree of this signal pulse sharpness that serves as the basis for one of the methods of fiber length discrimination used on the FAM. The general scattering function to be applied in this case is:[22]

$$S(Z, \phi) = \frac{kL}{\pi} \frac{\sin kLZ/2}{kLZ/2} T(\phi) \tag{14}$$

where Z is the angle between the scattering detection axis and the plane perpendicular to the fiber axis. For the geometry illustrated in Figure 3, Z can be expressed in terms of θ and ϕ by the relationship:

$$\sin Z = \sin \theta \sin \phi \tag{15}$$

Assuming ϕ to be nearly 90^{o}, to a close approximation equation (14) becomes

$$S(\theta, \phi) = \frac{kL}{\pi} \frac{\sin kL\theta/2}{kL\theta/2} \tag{16}$$

The scattering intensity or detected intensity is defined by:

$$I = I_{o} S^2/k^2r^2 \tag{17}$$

Replacing equation (16) in equation (17), and since $k = 2\pi/\lambda$ we obtain:

$$I = I_{o} \frac{L^2}{\pi^2 r^2} \left(\frac{\sin \pi L\theta/\lambda}{\pi L\theta/\lambda}\right)^2 T^2(\phi) \tag{18}$$

where $T(\phi)$ is a complex function of ϕ, m, λ and a_f.

The parameters of the above function are:

a_f = fiber radius

L = fiber length

m = fiber index of refraction at λ

λ = wavelength of illumination

θ = fiber axis angle in the plane of rotation
($\theta = 0$ is defined as broadside viewing of fiber axis)[23]

ϕ = scattering angle (90^{o} for the FAM)

r = distance between the fiber and the detector.

*Note: Van de Hulst's notation[22] was reversed for consistency with the notation previously used in this report.

For fibers whose diameter is larger than about 1/3 λ (approximately 0.2 μm for the He-Ne laser the scattering intensity increases as ϕ decreases, but for smaller diameter fibers $T^2(\phi)$ becomes nearly independent of ϕ.[23,24] Thus the use of forward scattering optics would not substantially improve the ability of the FAM to detect thin fibers but would result in added complexity of signal detection and interpretation. The function $T(\phi)$ will not be further analyzed because within the method selected for fiber length discrimination, the contribution from that function will be cancelled out as will be shown forthwith.

Assuming all parameters of equation (18) to be constant with the exceptions of fiber length L, and fiber angle θ, the intensity of the detected scattering signal in the vicinity of the maximum amplitude point of $\theta = 0$ is shown in Figure 4 for four different fiber lengths. It becomes apparent from this graph that as fiber length increases (all other parameters remaining invariant) pulse sharpness and amplitude increase concurrently. It further becomes obvious that for fibers longer than about 5 μm most if not all of the scattering signal is contained within a very narrow angle of rotation of less than about $\pm 6^{o}$ around the perpendicular or face-on position of observation, thus producing the above-mentioned search-light-like pulses.

Pulse Width Detection Method

One of the primary objectives of this development was to detect individual fibers and size-discriminate them in terms of length. During the early phases of this program several alternative methods for fiber geometry discrimination were investigated such as the detection of the phase angle between the applied field and the fiber axis, the ratio of the detected signal between side viewing and end-on viewing, sensing of the two polarization components, etc. It was concluded that all of the methods had serious drawbacks in that they provided mainly information on the length-to-diameter ratio of the fibers and/or the diameter, and in the case of the phase angle detection method this approach was only applicable to nonconductive fibers (see preceding discussion in this report), the method of end view to side view intensity ratio which is approximately proportional to the ratio L^2/λ^2 requires a very precise determination of the signal baseline (to within better than 1 percent), which is very difficult to achieve in the presence of nonfibrous particles in the sensing volume. Furthermore this method would be extremely sensitive to deviations of fiber shape from a perfect cylinder. The primary length discrimination method selected for incorporation in the FAM was based on the analysis of the angular scattering intensity distribution of each fiber as it undergoes its synchronous rotation. As mentioned before, two pulses of scattered light are observed for each complete fiber rotation, and a number of these pulses is detected as the fiber rotates through the sensing volume. The measurement of the widths or the sharpness of these pulses was considered to uniquely characterize their lengths as discussed within the preceding section on the light scattering behavior of acicular particles. The method of pulse width sensing has the advantages of: (1) independence from the electrical properties, the index of refraction (and the diameter of the detected fibers), (2) independence from the absolute intensity values both of the illuminating laser beam as well as the detector sensitivity, (3) relative simplicity of signal processing.

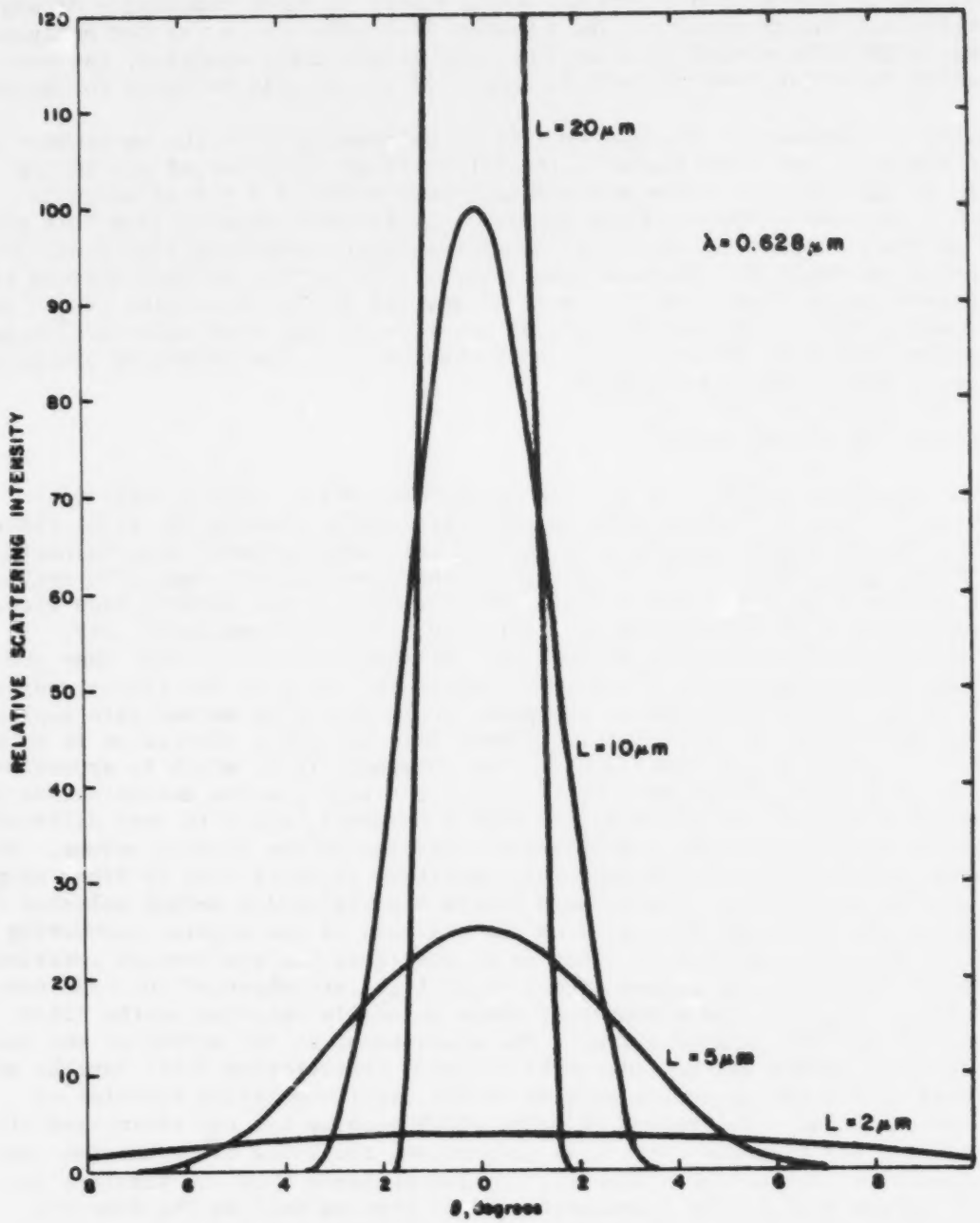

Figure 4. Pulse shape as a function of fiber length

Basically this method consists of sensing the detected pulse width at some specific fraction of its peak amplitude, thus normalizing each measurement against that peak value. Two main approaches were considered in order to implement this technique: sensing the ratio between the peak amplitude and the signal average, and sensing the ratio of the averages of the signals contained between two different rotation angle ranges. The first approach can be expressed mathematically as (from equation (18)):

$$\frac{I_{peak\ (\theta = 0)}}{I_{average\ (\theta < \theta < 2\pi)}} = \frac{I_o \frac{L^2}{\pi^2 r^2} T(\phi)}{I_o \frac{L^2}{\pi^2 r^2} T(\phi) \frac{1}{2\pi} \int_o^{2\pi} \left(\frac{\sin \pi L\theta/\lambda}{\pi L\theta/\lambda}\right)^2 d\theta} \tag{19}$$

$$= \frac{2\pi}{\frac{\lambda}{\pi L} \int_o^{2\pi^2 L/\lambda} \frac{\sin^2\alpha}{\alpha^2} d\alpha} \tag{20}$$

which for $L > 1$ μm and $\lambda = 0.628$ μm is essentially equal to:

$$\frac{I_{peak}}{I_{average}} = \frac{4\pi L}{\lambda} \tag{21}$$

Equation (21) indicates that this ratio is proportional to fiber length, λ being constant. The disadvantage of implementing this method, however, is that true pulse peak detection suffers from poor noise immunity. Thus the alternate method of pulse sharpness detection was pursued and incorporated in the final version of the prototype FAM. This technique consists of integrating each pulse train from a fiber using two different gate widths corresponding to two different intervals of θ. The first interval extends from the pulse center ($\theta = 0$) to a time τ_1 corresponding to an angle θ_1. The second gating interval extends from τ_1 to $2\tau_1$, or $2\theta_1$. In practice, this integration is performed symmetrically on both sides of the pulse center as illustrated in Figures 5 and 6. If the amplitudes of the pulses are proportional to the scattering intensities observed by the detector, then, from equation (18) the ratio, R, of the two pulse integrations is:

$$R = \frac{\int_o^{\theta_1} \left(\frac{\sin \alpha}{\alpha}\right)^2 d\theta}{\int_{\theta_1}^{2\theta_1} \left(\frac{\sin \alpha}{\alpha}\right)^2 d\theta} \tag{22}$$

where $\alpha = \pi L\theta/\lambda$

$\theta_1 = \omega\tau_1$, and

$\omega = d\theta/dt$

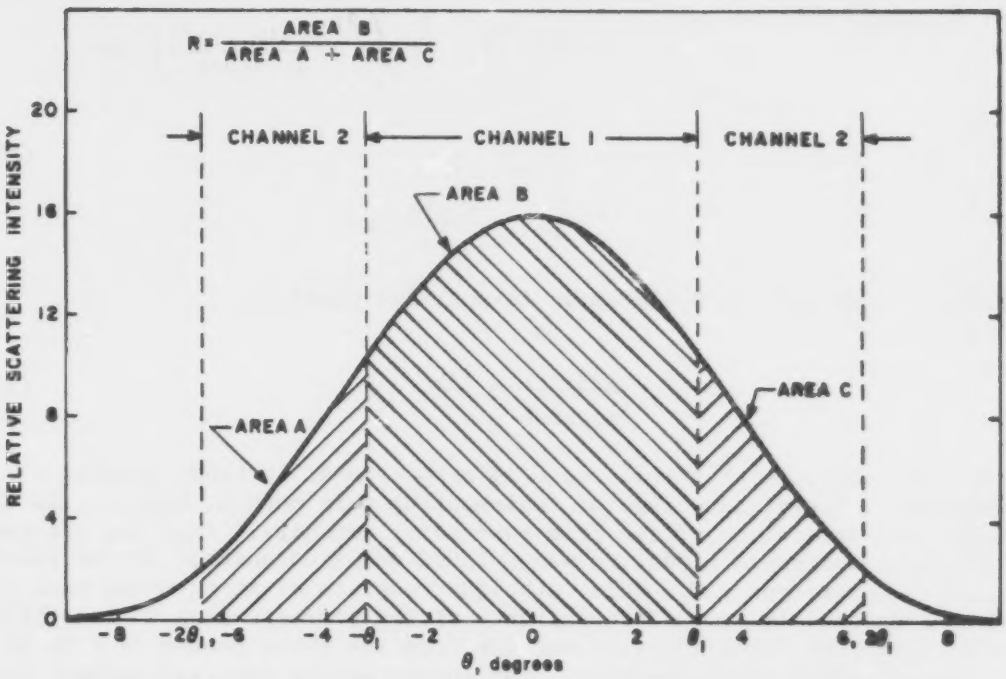

Figure 5. Detection pulse shape for a 4 μm long fiber (λ = 0.6328 μm) and gating intervals for the ratio method of fiber length determination

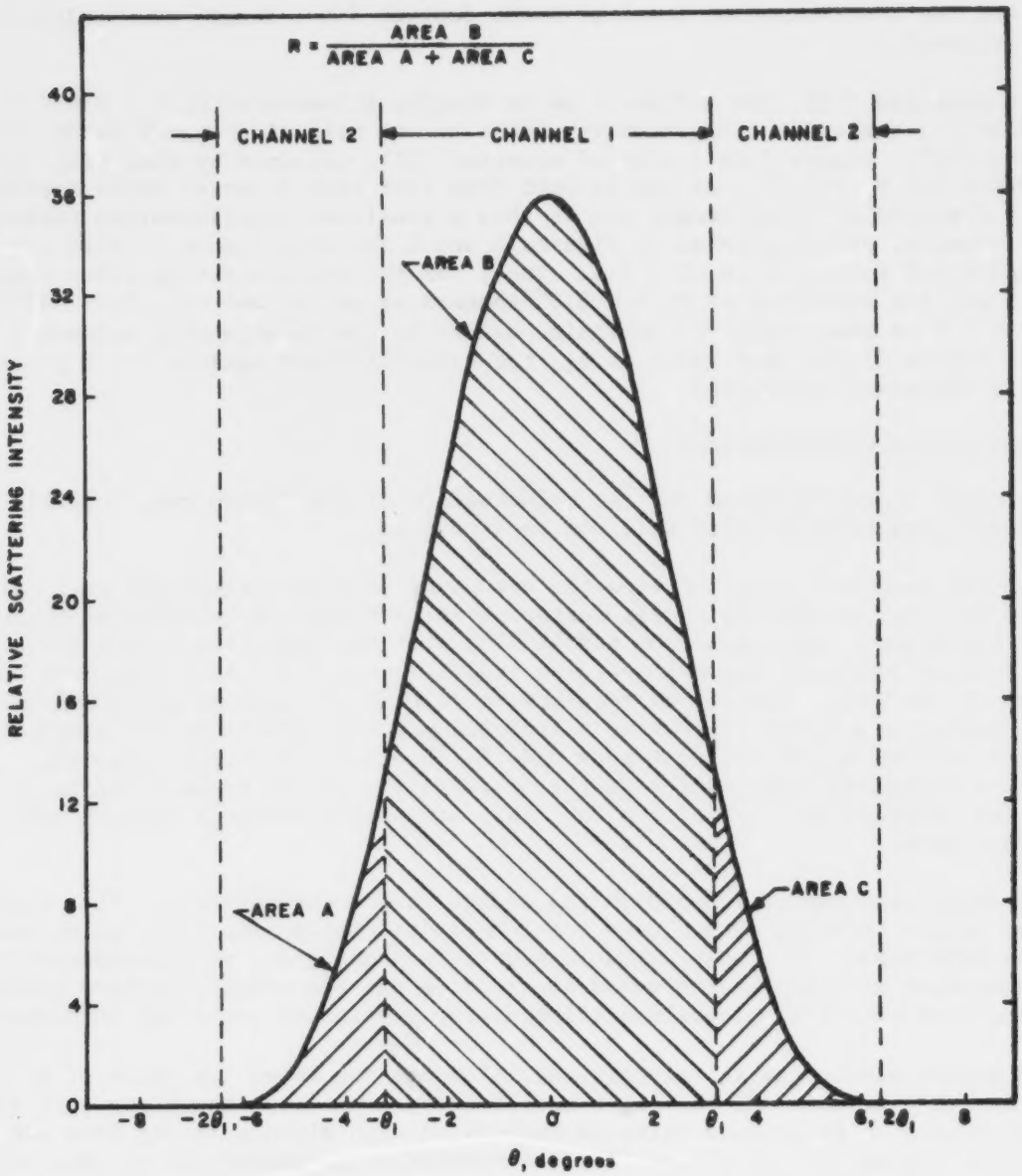

Figure 6. Detection pulse shape for a 6 μm long fiber (λ = 0.6328 μm) and gating intervals for the ratio method of fiber length determination.

From equation (22) it is evident that R is only a function of L for a constant value of λ, the wavelength of illumination. In practice R is obtained by averaging electronically over each complete pulse train associated with a discrete fiber passage through the sensing volume. By the appropriate choice of θ_1 and the discrimination level of R the desired fiber length discrimination is achieved.

From equation (18), for a fiber 5 μm in length, illuminated by $\lambda = 0.632$ μm radiation, the scattering intensity drops to one half of the peak value when $\theta = \pm 3.2^{o}$. Figure 7 is a plot of equation (22), obtained by numerical integration for $\theta_1 = 3.2^{o}$. As can be seen from that plot R varies quite rapidly as a function of fiber length and is thus a sensitive discrimination parameter. For example, as illustrated on Figures 5 and 6 and from Figure 7, with L = 4 μm, R = 2.4 and for L = 6 μm, R = 7.4. Thus, for the discrimination fiber length of 5 μm, the selection of $\theta_1 = \pm 3.2^{o}$ appears as an optimal solution. Although for L > 8 μm some degree of ambiguity exists in the relationship between R and L (see Figure 8) for that value of θ_1, the discrimination against L < 5 μm remains obviously unaffected.

Light Source Considerations

The light source required for the illumination of the fibers must fulfill several requirements which will now be discussed.

From the geometric point of view the beam must be nondivergent and well collimated in order to provide a well-defined sensing volume of cylindrical shape. Any significant departure from parallelism over the detection length would resulr in occasionally incomplete pulse trains when a fiber is moving near the edge of the beam. The second requirement is that the beam be polarized and that the radiation electric vector be positioned perpendicularly to the scattering plane defined by the incident beam and the observed scattering direction. The use of polarized light source further permits the use of Brewster-angle windows on the sensing-flow duct of the FAM, thus minimizing spurious reflections at such windows.

The third requirement imposed on the source is monochromaticity. This requirement arises from the method used for length discrimination; i.e., pulse sharpness detection. If a polychromatic source is used (e.g., an incandescent lamp) a continuum of pulse widths would be produced and the sharply defined pulses associated with a single-valued illuminating wavelength could not be observed.

The source wavelength is not critical, although the lower the value of λ, the higher the intensity of the light scattered by a Mie-type scatterer. If the main source of background noise is associated with Mie-scattering from non-fibrous shaped dust particles (i.e., a reasonable approximation to this case) then, as a first order approximation, shorter wavelengths result in higher signal-to-noise ratios.

The light intensity within the detection volume determines, among other parameters, the signal-to-noise ratio because the signal amplitude is directly proportional to the intensity of illumination, whereas the noise (being mainly

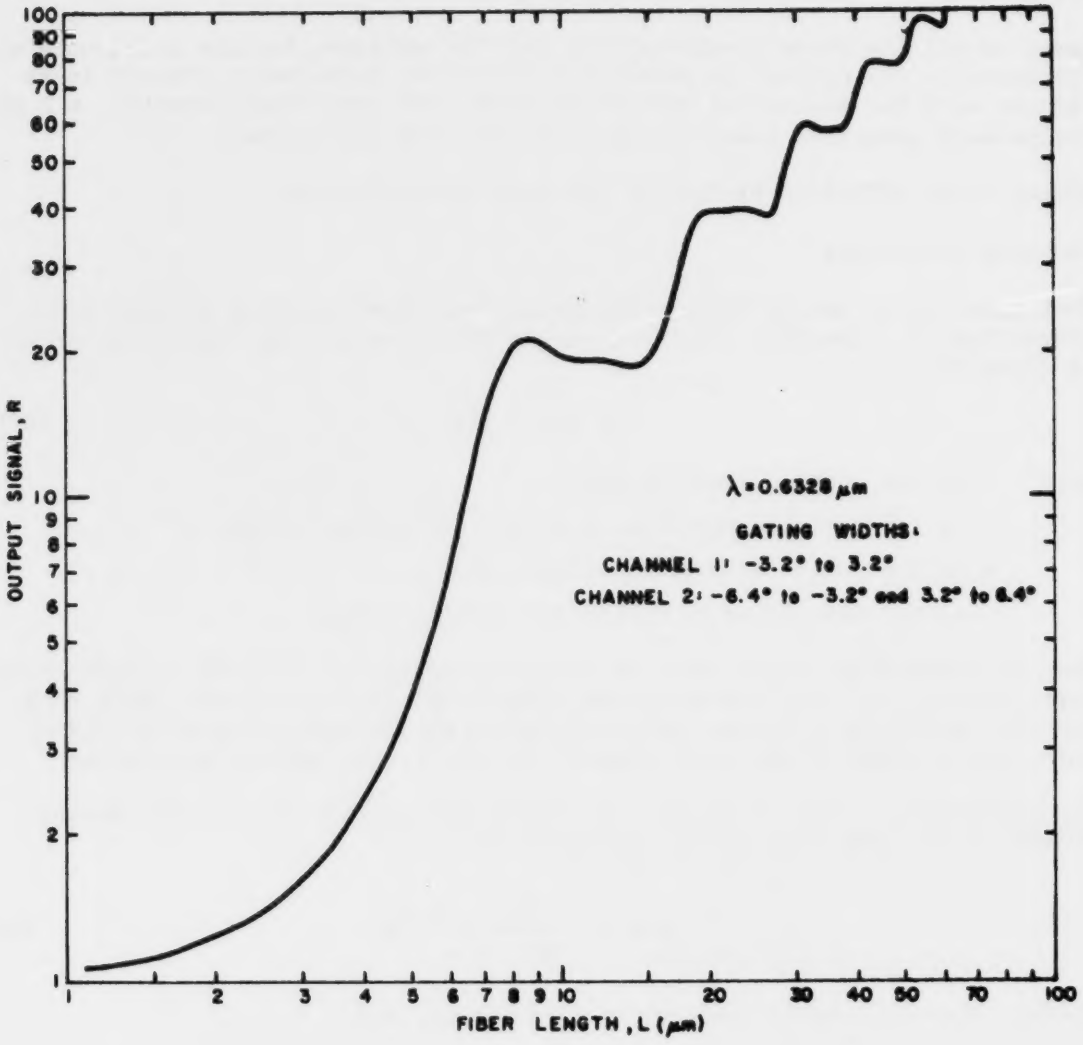

Figure 7. Ratio signal as a function of fiber length

of the shot noise type) is proportional to the square root of the light intensity. Thus, beam expansion would result not only in an increase in fiber detection coincidence errors but also in diminished signal-to-noise ratios.

Last but not least, cost, availability, size, weight and power consumption were important selection criteria imposing stringent limitations on candidate light sources.

Based on all the above considerations and, in addition, because continuous wave illumination (as opposed to pulsed operation) was required to prevent interference with the scattering modulation associated with fiber rotation, a 2 mW helium-neon polarized laser was selected for this application.

SINGLE FIBER DETECTION STATISTICS AND FLOW CONSIDERATIONS

Counting Statistics

Each fiber as it passes through the detection volume produces a pulse train consisting of a specific number of pulses whose number (per individual fiber) is given by:

$$\eta = 2f\tau = 2fxv \tag{23}$$

where f is the applied field frequency,

τ is the particle residence time in the sensing volume,

x is the length of sensing volume, and

v is the flow velocity within the sensing volume.

Each of these pulse trains must be detected separately in order to sense discrete fibers, and thus the detection volume must be sufficiently small such that for the highest number concentration to be measured the probability of more than a single fiber being present in this volume remains negligible.

The probability P that N events (or fibers) are present within the sensing volume at the same time can be expressed by:

$$P(N) = \frac{(C\,V_s)^N}{N!}\, e^{-C\,V_s} \tag{24}$$

where C is the number concentration of fibers, and

V_s is the sensing volume.

The total probability of particle coincidence is the sum $\sum_{N=2}^{N=\infty} P(N)$. As a useful practical rule, however, if the sensing volume is smaller than the one-half of the inverse of the maximum particle concentration the total coincidence error is less than about 10 percent.

The statistical accuracy of the counting process follows reasonably well a Poison-type distribution and thus the relative standard deviation ε_r of the fiber count can be calculated from:

$$\varepsilon_r\ (\%) = \pm \frac{\sqrt{c}}{c} \times 100 \tag{25}$$

where c is the total fiber count over a sampling period T and thus

$$c = \frac{TCV_s}{\tau} \tag{26}$$

The program objectives were stipulated in terms of ε_r, T and C and thus V_s and τ became the variable design parameters of the FAM.

Flow Considerations

One of the primary requirements for the selective detection of fibrous-shaped particles is that the flow within the sensing region be totally devoid of turbulence, and in addition the flow stream must be parallel to the illuminating light beam; i.e., the axis of the sensing volume. Furthermore it is preferable that the velocity of all streamlines within the sensing volume be the same and that no acceleration or deceleration of the flow velocity occur within this volume. These conditions can be met with a fully developed parabolic laminar flow profile if the sensing volume is constrained to a small radius (as compared to the duct radius) centered on the flow axis. The requirement for laminar flow conditions within the sensing volume results from two detection aspects: (a) fiber motion must be rectilinear in the direction of flow and purely rotational in the perpendicular plane in order to preserve the signal pulse shape, and (b) fibers cannot be allowed to drift in and out of the sensing volume thus producing incomplete pulse trains. From the experimental evidence found during the initial phases of the FAM laboratory investigation, it was found that a low Reynolds number (< 500) based on the duct diameter, is by itself an insufficient criterion for flow stability. Flow obstructions, discontinuities and short inlet lengths can produce unacceptable instabilities that are reflected in signal breakup and distortions.

RECTILINEAR AERODYNAMIC BEHAVIOR OF AIRBORNE FIBERS

General Theory for Ellipsoids of Revolution

The theoretical aspects of the rectilinear aerodynamic behavior of fibrous-shaped particles were explored within this program in order to provide guidelines for the use and selection of respirable versus nonrespirable size separation methods. The rotational aerodynamic behavior of fibers was treated in a preceding section of this report as related to the motion imparted to the fibers by the applied rotational electric field.

In general, the dynamic behavior of all aerosol particles is governed by their aerodynamic properties; i.e., their motion is the resultant of opposing forces: a driving force such as gravitational acceleration, and the viscous resistance

of the medium within which the particle moves. In this context, highly useful characterization is that of aerodynamic equivalent diameter or Stokes diameter, defined as that diameter of a sphere of unit density whose settling velocity equals that of the particle under consideration. In the case of acicular particles this settling velocity depends on particle orientation with respect to the direction of motion.

The treatment to be followed on aerodynamic characterization and that of the preceding section on the electrodynamic behavior are based exclusively on the assumption that the fiber motion is in the Stokes regime and no attempts are made to incorporate slip corrections (Cunningham) in these calculations since no adequate treatment of such regime has been developed for particles other than spherical. It is, however, to be expected that for fiber diameters of less than about 0.5 μm, especially when the fiber motion is parallel to its axis, the aerodynamic properties will no longer be correctly characterized by a purely Stokes treatment. In this context it is worth mentioning that the FAM may be developed into a tool for the experimental investigation of slip correction factors for acicular particles.

The Stokes regime can be characterized by the condition wherein the resistance to motion within the fluid is purely viscous; i.e., the Reynolds number is typically less than 0.5, resulting in a symmetrical distortion of the fluid upstream and downstream of the particle, without wake asymmetry. The drag equation for spherical particles is well known under these conditions. Even cylindrically shaped fibers require a somewhat more elaborate treatment. A mathematical approximation to an ellipsoid of revolution appears as a reasonable approximation,[20] which has also been applied to model the deposition of fibers in the human respiratory system.[29] Two extreme cases can be recognized: (1) motion of the ellipsoid (or fiber) along its axis of revolution, and (2) motion perpendicular to the axis of revolution. It should be considered that the gravitational settling motion of any particle with three mutually perpendicular planes of symmetry (such as an ellipsoid of revolution) will be invariant during its descent, maintaining its initial orientation through its fall trajectory. In practice, however, asbestos fibers for example may not always be perfectly straight and the above-mentioned rule can be violated.

As noted above, acicular particles can be approximated by ellipsoids of revolution falling under the action of gravity in either of two attitudes described under (1) and (2), or any intermediate angle with respect to the direction of motion. In general, an acicular particle falling with its axis vertical will have a higher terminal velocity than the case when its axis is normal to the direction of motion. Intermediate angles will exhibit intermediate velocities. The difference between cases (1) and (2) are, however, not as significant as intuition would indicate. Two equations represent the two extreme axis-to-motion angles defined above.

$$\text{For case (1): } D = \frac{4/3\ d}{\frac{2\beta^2-1}{(\beta^2-1)^{3/2}} \operatorname{arc\,cosh}(\beta) - \frac{\beta}{\beta^2-1}} \qquad (27)$$

and for case (2): $$D = \frac{8/3\ L}{\frac{2-3\beta^{-2}}{(1-\beta^{-2})^{3/2}} \text{ arc cosh } (\beta) + \frac{1}{1-\beta^{-2}}} \qquad (28)$$

where D is the diameter of the sphere having the same settling velocity.

Equations (28) and (29) are plotted on Figure 8,[20] curve i) refers to the ellipsoid of revolution moving in the direction of its axis of rotation, and curve ii) refers to the case when the motion is at right angles to the axis.

Once the value of D has been determined for a given particle, and provided that the particles fall vertically (no lateral glide) and do not change their orientation during their vertical motion, D can be replaced in the classical Stokes equation for the diameter of a spherical particle:

$$V_s = \frac{(M_p - M_g)g}{3\pi\ \eta D} \qquad (29)$$

where V_s is the settling velocity

M_p and M_g are the masses of the particle and the displaced gas,

respectively (M_g is usually negligible)

g is the acceleration of gravity

D is the diameter of the spherical equivalent particle

η is the gas viscosity

An an example, the fiber dimensions will be assumed to be:

diameter = 0.1 μm

length = 5 μm $\quad \beta_i = 50$

Based on a density of asbestos fiber of 2.6 g/cm^3, the viscosity for air at standard conditions of 1.8×10^{-4} poise, the determination of settling velocity is performed as follows:

Case i):

Referring to Figure 8, curve i), we find a value of D/d = 8 for $\beta = 50$. Therefore D = 0.8 μm.

The particle mass is:

$$M_p = \frac{\pi}{4}\, 0.1^2 \times 10^{-8} \times 5 \times 10^{-4} \times 2.6 = 1.02 \times 10^{-13} \text{g}$$

Replacing M_p in equation (29) we obtain $V_{s(i)} = 7.4 \times 10^{-4}$ cm/sec.

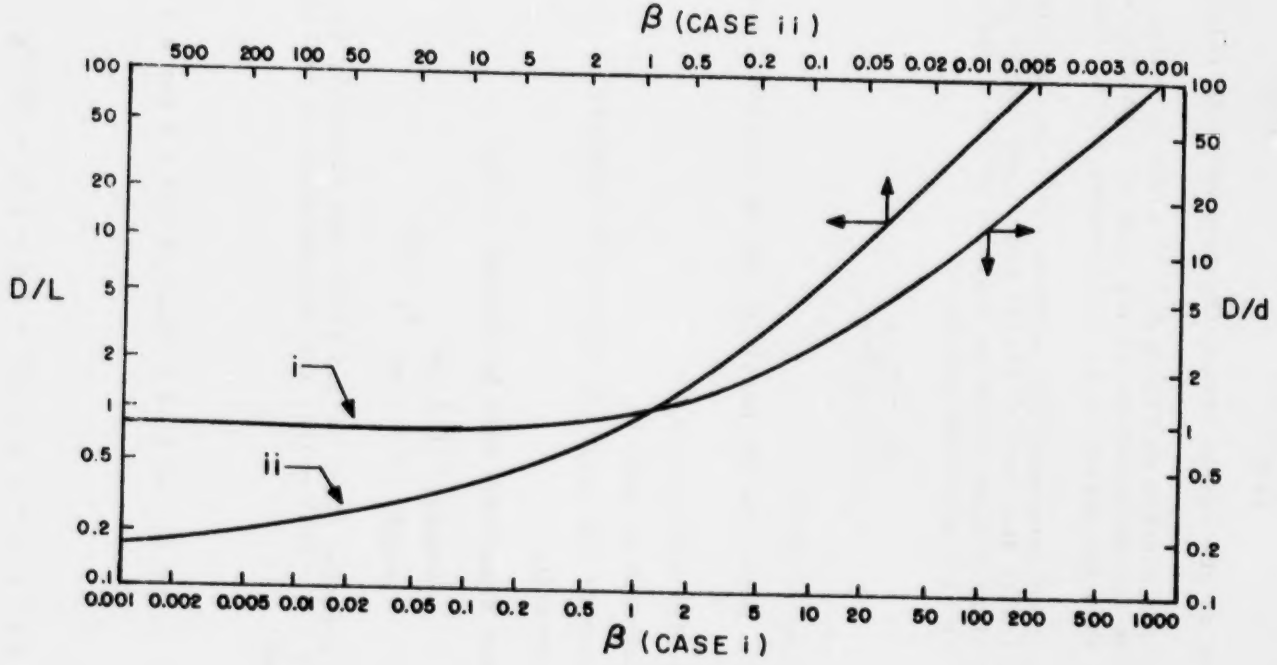

Figure 8. Sedimentation of ellipsoids, i) axis parallel to direction of motion; ii) axis normal to direction of motion.[20]

Case ii): In this case $\beta_{ii} = \frac{1}{\beta_1}$

Referring to Figure 8, curve ii), the value of D/L = 0.27 is found for β_{ii} = 0.02, thus D = 1.35 μm, thus $V_{s(ii)} = 4.4 \times 10^{-4}$ cm/sec.

One of the important conclusions to be reached from the preceding calculations is that the settling velocity of fibers does not vary more than about a factor of 2 whether the fiber falls with its axis aligned vertically or horizontally (this also applies to larger particles than the above example). Since in most real cases deviation from true ellipsoidal shape will preclude perfect vertical or horizontal trajectories, a good practical rule for the calculation of settling velocities of fibers is to average the results obtained for the two extreme particle orientations. For the above example, the average would be 5.9×10^{-4} cm/sec.

Another aspect to be considered in the context of the aerodynamic behavior of acicular particles is their orientation within a flow field as a result of shear forces exerted by the moving fluid. Although, as noted previously, an acicular particle (rigorously an ellipsoid) tends to fall without rotation in a gravitational field, in the case of a laminar flow through a duct, these particles tend to align with their long axis with the direction of flow. This is a result of the transverse velocity gradient in a fully developed laminar flow (i.e., with a parabolic velocity profile) which causes a torque on the elongated particle until alignment with the direction of flow is attained. As applied to the FAM, this means that fibers arriving at the sensing volume will, most probably, be aligned with the flow direction before being oriented within the quadrupole field.

Respirable Fiber Segregation

The penetration of fibrous-shaped particles into the lower respiratory passages is determined by their aerodynamic properties.[29] Therefore methods for fiber size selection or precollection are preferably based on these properties. Although, as demonstrated within the preceding analysis, the effect of fiber orientation on their aerodynamic behavior is limited to factors of the order of 2, it can be concluded that such a size selection should be performed within the laminar flow regime in order to fully define the orientation of the fiber prior to their aerodynamic segregation. Thus, centrifugal flow fields, especially those associated with cyclone collectors do not fulfill this condition. Furthermore these devices, due to their high velocity gradients may lead to fiber break-up and reentrainment. The lack of fiber size segregation definition of cyclones has been reported[30] indicating that a sampling flow range as large as 1.1 to 1.9 liters/min resulted in approximations to the ACGIH Respirable Dust Curve. Horizontal or vertical elutriation can, however, be effected within the laminar flow regime. Horizontal elutriation, although used as a standard method of precollection for nonfibrous dusts such as coal mine dust, has the potential disadvantage of particle reentrainment from the collection surfaces. Vertical elutriation appears as the most compatible solution for the retention of nonrespirable fibers whose aerodynamic size exceed a minimum particle cut-off. Laminar flow conditions are usually encountered in such devices; e.g., the 7.4 liter/min elutriator proposed as a standard method for cotton dust sampling operates at a Reynolds number of approximately 100 with a particle cut-off Stokes diameter of 15 μm.[31,32] The

particular cut-off size for fibrous aerosols such as asbestos remains to be determined. The flow laminarity within a vertical elutriator results in a parabolic velocity profile with a continuum of velocities ranging from zero at the wall of the duct to twice the average velocity at the axis. It is thus inevitable that the particle cut-off characteristic of such a device will be rather broad, a fact which is probably compatible with the retention characteristics of the human respiratory system.

PROTOTYPE INSTRUMENT DEVELOPMENT

LABORATORY TEST SYSTEM

Experimental "Breadboard"

One of the earliest tasks within this instrument development program was to set up an experimental system which could be used as a test "breadboard". This set-up was then to be modified and optimized in order to determine empirically the design parameters to be implemented in the final prototype instrument design and fabrication. Several of these "breadboards" were assembled and tested during the initial phases of the program and as a result of the difficulties encountered and the experience gained from the operation of these test devices a preferred design emerged.

The experimental breadboard consisted of the optical illumination train, the flow tube-quadrupole assembly, the light scattering detector, and the auxilliary circuitry for the generation of the rotational field and for signal detection. The final optical and flow-detection breadboard configuration was essentially identical to that of the two identical prototype instruments delivered at the completion of the program and will thus be discussed in detail within the section of this report describing the final instrument design. The intermediate developmental steps are obviously only of anecdotal interest and will not be detailed within this report. The only basic difference between the final breadboard version and the completed instruments was that the former was supported by a large bench-top optical table with magnetic latches whereas the latter used a special honeycomb-type structural panel for the support of the optical components.

Among the developmental steps of more than passing interest, however, it is worth mentioning the following ones. The quadrupole electrode configuration underwent a series of design modifications dictated by flow stability considerations (see preceding section of this report) and by surface contamination problems when these electrodes were placed on the exterior surface of the transparent flow duct. The optical system underwent a number of evolutionary modifications: midway through the program it was considered that a laser beam expander followed by a stop and re-imaging optics would be required to provide a squared-off beam at the sensing volume. The need for these elements was later obviated by the method of pulse width detection, and in addition, as it was established that maximum beam intensity resulted in optimum signal-to-noise ratios.

The quadrupole field generator circuit initially employed for the early testing efforts consisted of the elements depicted in Figure 9. The oscillator was a Hewlett Packard Model 200 CD and the two amplifiers were part of a Realistic

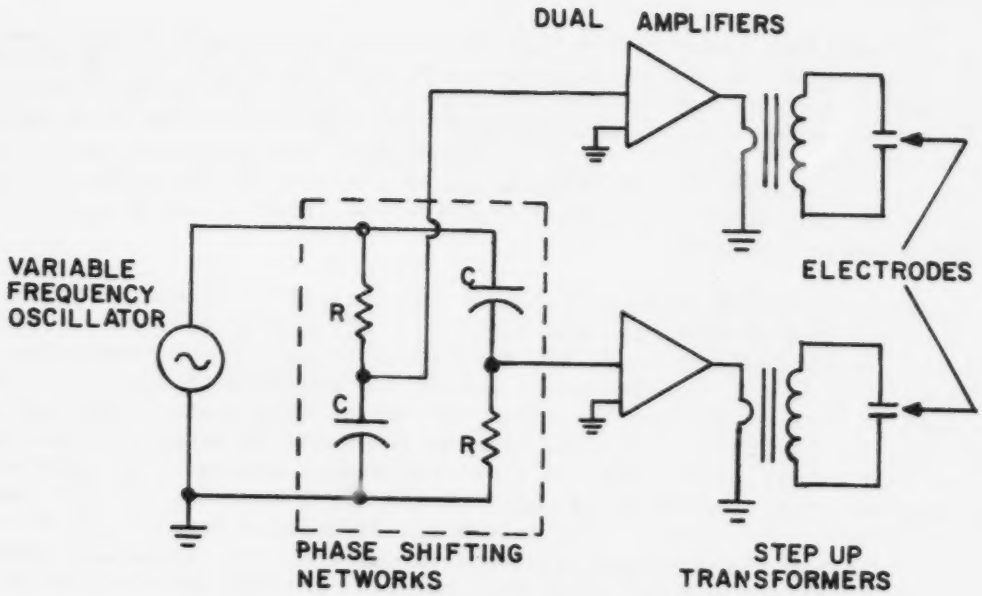

Figure 9. Schematic of initial version of the circuitry used to generate rotating electric field

Model SA-10 stereo unit with an output power of about 1 watt per channel. Two power transformers were used as step-up transformers and the final field potential thus obtained was obtained 1800 V peak-to-peak. The two complementary RC circuits were used to produce the desired 90^{o} phase shift between the two voltages. The final version of the field generating circuit will be described further ahead in this report.

The signal detection system used with the laboratory breadboard consisted of an integral photomultiplier-high voltage supply-dynode divider to be discussed in more detail within the instrument description, followed by Princeton Applied Research HR-8 Lock-in amplifier and/or a direct oscilloscope display using one of the quadrupole waveforms as horizontal trigger, in order to discern the pulse trains associated with the detection of discrete fibers. Final testing and system optimization were, however, performed using the complete advanced signal processing circuit developed for the portable prototypes.

Flow Tests

Early during the developmental efforts it had been determined, as mentioned previously, that flow laminarity was a condition *sine qua non* for the successful operation of the FAM. In order to achieve fully developed flow laminarity the following conditions had to be fulfilled in addition to the usual low Reynolds number criterion (less than about 1000 for a duct consisting of several sections with some degree of interfacial discontinuity): (a) inlet diameter comparable to duct diameter, (b) duct length (from inlet to sensing volume) to duct diameter ratio exceeding about 12 for the selected diameter of 1 cm and flow rate of 2 liters/minute, (c) absence of any obstructing elements in the flow duct upstream of the sensing region, and (d) absence of any measurable leaks at any point within the flow-sensing duct leading to flow distortions.

The above requirements and the actual flow laminarity were confirmed experimentally using the smoke injection method depicted in Figure 10. The test aerosol (cigarette smoke) was injected axially with a hypodermic needle into a 1 cm ID glass tube and a high intensity lamp was used to axially illuminate the entire volume of the tube. At low flow velocities entering through the right-angle inlet bend, the injected smoke was observed as a thin straight line traversing the length of the tube parallel to the duct axis. When using an inlet diameter of about 0.48 cm (i.e., less than one-half the flow duct diameter), onset of turbulence was clearly observed even at a duct Reynolds number of only about 130. By increasing the inlet diameter to 1 cm laminarity at the sensing region was preserved up to a Reynolds number of 400 corresponding to a flowrate of about 3 liters/minute through the 1 cm diameter flow tube; i.e., well in excess of the 2 lpm design objective.

Fibrous Aerosol Generation

The successful development of the FAM was contingent on the reliable laboratory generation of fibrous-shaped aerosol particles. It had been assumed, perhaps naively, that the stable and repeatable production of such aerosols with discrete nonagglomerated fibers at typical concentrations of a few fibers per cubic centimeter was an easily achievable objective. As it became apparent that these conditions of generation were extremely difficult to obtain with the commonly available methods of aerosolization, an increasing and sustained

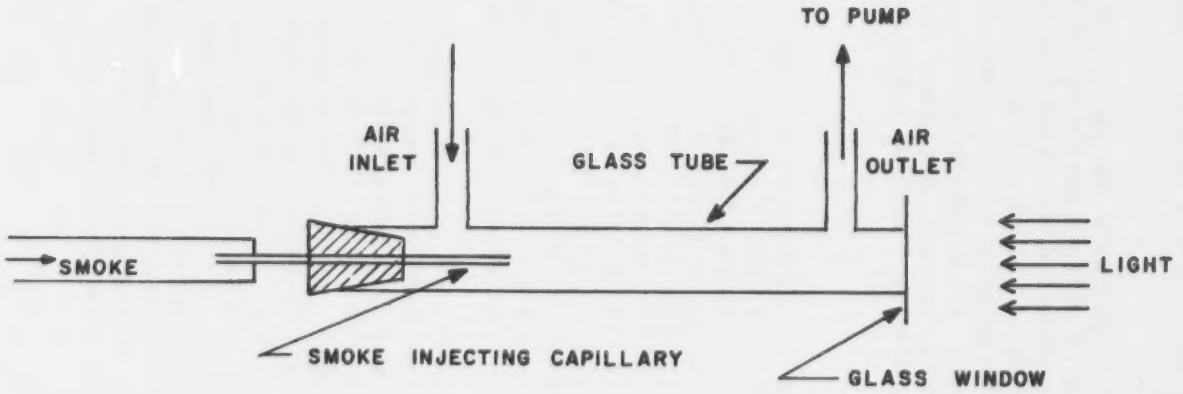

Figure 10. Flow test system used to observe air flow streamlines. The glass tube was 25 cm in length with a 1 cm I.D.

effort had to be expended in order to develop the required methodology and instrumentation required to produce a useful fibrous test aerosol. The successful development of a simple and at the same time reliable generator should be considered an extremely useful byproduct of this program.

Initially all tests were performed using aerosol generation by atomization or nebulization from a hydrosol suspension of asbestos in water. The use of a Collison Generator resulted in frequent and usually rapid clogging of the small orifices of that device, and consequently a glass De-Vilbiss No. 40 pharmaceutical nebulizer was used for the initial experimental effort.

Freshly prepared 0.01 percent (by weight) aqueous crocidolite hydrosols were thus aerosolized to provide straight test fibers. When this aerosol was introduced into the laboratory breadboard of the FAM and the detected signals were displayed on an oscilloscope it was consistently observed that the number concentration of long fibers, as characterized by pulse trains consisting of narrow pulses of large amplitude, decreased noticeably as a function of time (of the order of a few minutes) elapsed from the start of the generation process. Concurrently, an increase in the number of broad pulse trains, associated with short fibers, was observed. Eventually a point was reached when the signal resulting from these short fibers no longer consisted of separate pulse trains typical of discrete particles but became a continuous background signal. These observations, repeated at several different times, strongly indicate that the aerosol fiber generation process by nebulization gradually breaks up the longer fibers either at the point of generation; i.e., the nozzle, or upon impact of the larger droplets against the nebulizer wall.

To confirm these observations the experiment was repeated by collecting a sample of the fibrous aerosol on a 37 mm type AA Millipore filter. Three consecutive filter samples were thus obtained, one during the first 10 minutes of generation, one during the second 10 minutes, and the last during the third 10 minutes. Fiber counts were made for the first and last filters thus obtained, following the NIOSH method of phase contrast microscopy, with the modification that both fibers with length L less than 5 μm but with aspect ratios greater than 3:1 and exceptionally long fibers were also counted and categorized. This entire experiment was repeated twice. The first time an equal number of viewing fields from the first and last filter were compared. The second time the total number of fibers counted on the first and last filter was kept constant. These results are summarized in Tables 1 and 2 and although the fiber counts were statistically insufficient, these results can be considered as qualitative confirmation of the results obtained with the FAM breadboard.

It became evident from these tests that the FAM even in that partially complete state of development was an extremely useful tool for the detection and real-time analysis of fibrous aerosols and provided some heretofore unsuspected information on generally-accepted methods of generation. These tests also suggested that the development and testing of the FAM system required a more reliable and stable method of fibrous aerosol generation capable of providing unagglomerated particles at concentrations of up to 20 or 30 cm^{-3}.

Table 1. Comparison of fiber lengths as a function of nebulizer operation generation time. A total of 60 fields were observed for each filter.

Time period after start-up	Number of fibers		
	L < 5 μm	5 μm < L < 37 μm	37 μm < L
Initial 10 minutes	41	16	2
Final 10 minutes	31	8	0

Table 2. Comparison of fiber lengths as a function of nebulizer operation time. A total of 51 fibers were observed for each filter.

Time period after start-up	Number of fibers		
	L < 5 μm	5 μm < L < 37 μm	37 μm < L
Initial 10 minutes	36	13	2
Final 10 minutes	42	8	1

Fiber break-up in the nebulizer furthermore prevented the generation of any fibers whose length exceeded about 8 μm as indicated by microscopy of collected samples, although the suspension itself (before nebulization was started) was observed to contain numerous fibers exceeding 40 μm in length. Other methods of generation were tested, among them the spinning disc technique, but significant fiber agglomeration was generally observed. Before the FAM operating parameters could be adjusted and optimized it was imperative to generate reliable signals associated with discrete straight fibers. The gating angles or phase angles of the instrument could only be adjusted to their proper values with that type of fibrous aerosol. Thus the reliable generation of such discrete, fibers of length greater than 5 μm had to be achieved.

Two methods of dry generation of fibrous aerosol were considered at that time: the first was the technique described by Timbrell[33] and others, utilizing a plug of asbestos continuously fed into a rotating blade; the second method discussed by Spurny[34] involved the use of a fluidized asbestos (or fibrous dust in general) bed subjected to low frequency vibrations.

In order to evaluate the applicability of the first method to the test requirements of the FAM, a visit was made to Dr. David Hemenway at the Civil Engineering Department of the University of Vermont. A rotating blade device obtained in England was being utilized by the above-mentioned group in Vermont. This device consists of an asbestos plug slowly fed into a rotating blade in the standard manner used by Timbrell,[31] and Ortiz.[35]

The asbestos (chrysotile UICC) from the generator was fed into a vertical elutriator made from acrylic and of dimensions of approximately 0.3 m × 1 m × 1 m. The output of this elutriator was then fed into a second acrylic chamber of approximate dimensions 0.6 m × 1 m × 1 m high containing a fan. This chamber was used to damp out any variations in generation rate and to further break up the fibers.

The output of this generator was sampled and collected on a Nuclepore filter and subsequently coated with a thickness of a few Angstroms of platinum for observation with a scanning electron microscope.

The asbestos aerosol thus generated was found to be inadequate for the FAM testing requirements because of excessive fiber agglomeration. It was then decided to investigate the use of the fluidized bed approach because of its inherent simplicity. A small vibrating table was constructed as depicted in Figure 11. A vibrational amplitude of 0.75 mm peak-to-peak defined by the eccentricity of the drive shaft was established. The vibrational frequency was made variable from 0 to 40 Hz by adjustment of the voltage applied to the small d.c. drive motor. The fluidized bed consists of a 1.2 cm diameter filter on which a layer of about 0.5 cm thickness of the fibrous-material to be dispersed is placed. The flow rate through the bed was adjusted to result in an upward velocity of about 0.5 to 1.5 cm/sec, corresponding to the settling velocity of unity density spheres of 12 μm and 22 μm in diameter, respectively. As shown in Figure 11, the flow containing the fibers was diluted with either room or filtered air in order to obtain the total flow rate of about 2 liters/min required for the operation of the FAM. Most of the work was performed at a vibration frequency of the generator of 35 Hz and a flow rate of 50 cm^3/min (0.7 cm/sec).

Fiber Reference Counting

The concentration of airborne asbestos fibers during the FAM tests was determined by the NIOSH method[7] as described in a manual prepared by the NIOSH Division of Training. Salient features of this method are that Millipore type AA membrane filters, used to collect the aerosol, are cleared for transmission optical microscopy by dissolving a filter wedge with a solution of dimethyl phthalate and diethyl oxalate on a glass slide under a cover slip, and examining the now transparent filter with a phase-contrast microscope at approximately 450X magnification to determine the number of fibers greater than 5 μm in length. Sizing of the fibers is accomplished by the use of a Porton reticule, which is simply a rectangle with a series of circles the areas of which double from one circle to the next larger circle, that is scribed on one of the ocular lenses of the binocular microscope. The Porton reticule, in turn, is calibrated by comparing the circles with a stage micrometer, which is a microscopy slide that has 0.01 mm (10 μm) lines etched on it. For some of the comparison tests between the FAM and the NIOSH sampling method, fibers were characterized as less than 5 μm in length, or greater than 12.5 μm in length. All fibers with an aspect ratio (length to width ratio) of less than 3:1 were not counted.

The microscope used for fiber counting was an American Optical Microstar 10 outfitted with an Ortho-Illuminator light source, a phase condensor, green filter, and 40X phase objective. Photomicrographs were attainable by use of a Polaroid camera attachment to the microscope.

PROTOTYPE DESIGN

Optical System

Figure 12 is a schematic illustrating the optical configuration of the final version of the FAM prototype. Figure 13 is a photograph of the actual components

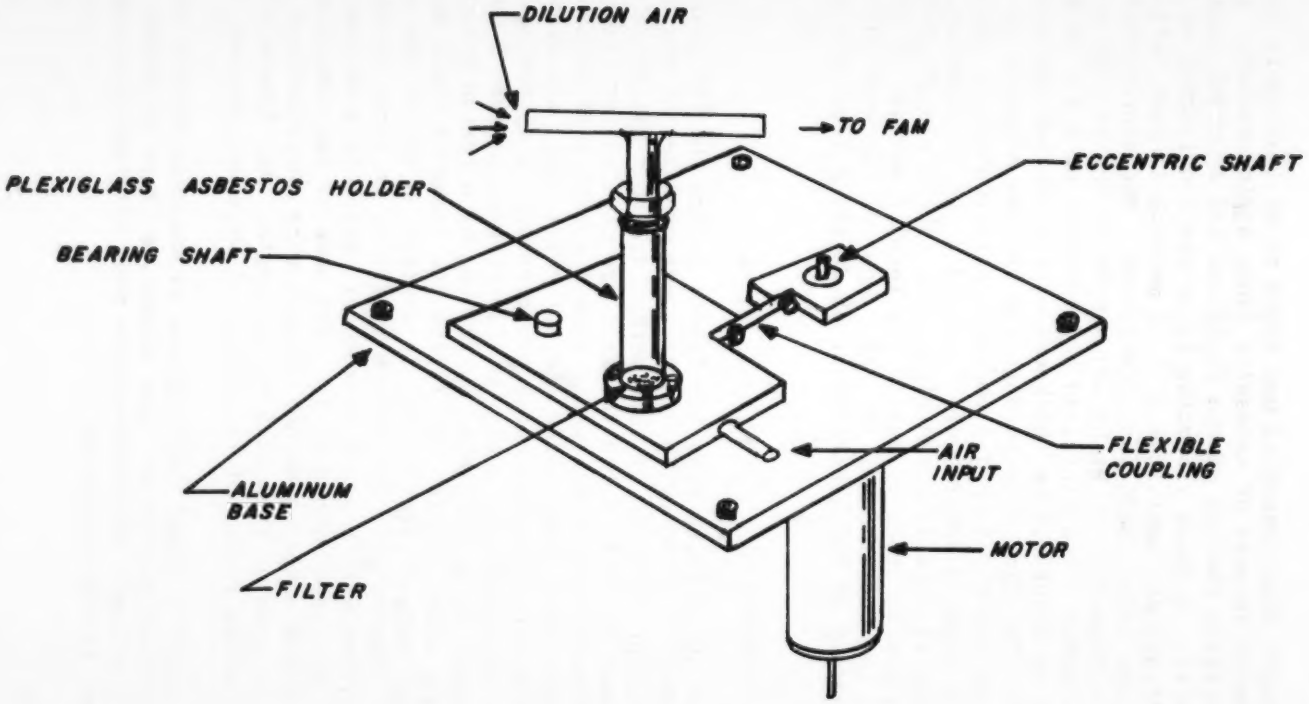

Figure 11. Hydrolized bed aerosol generator

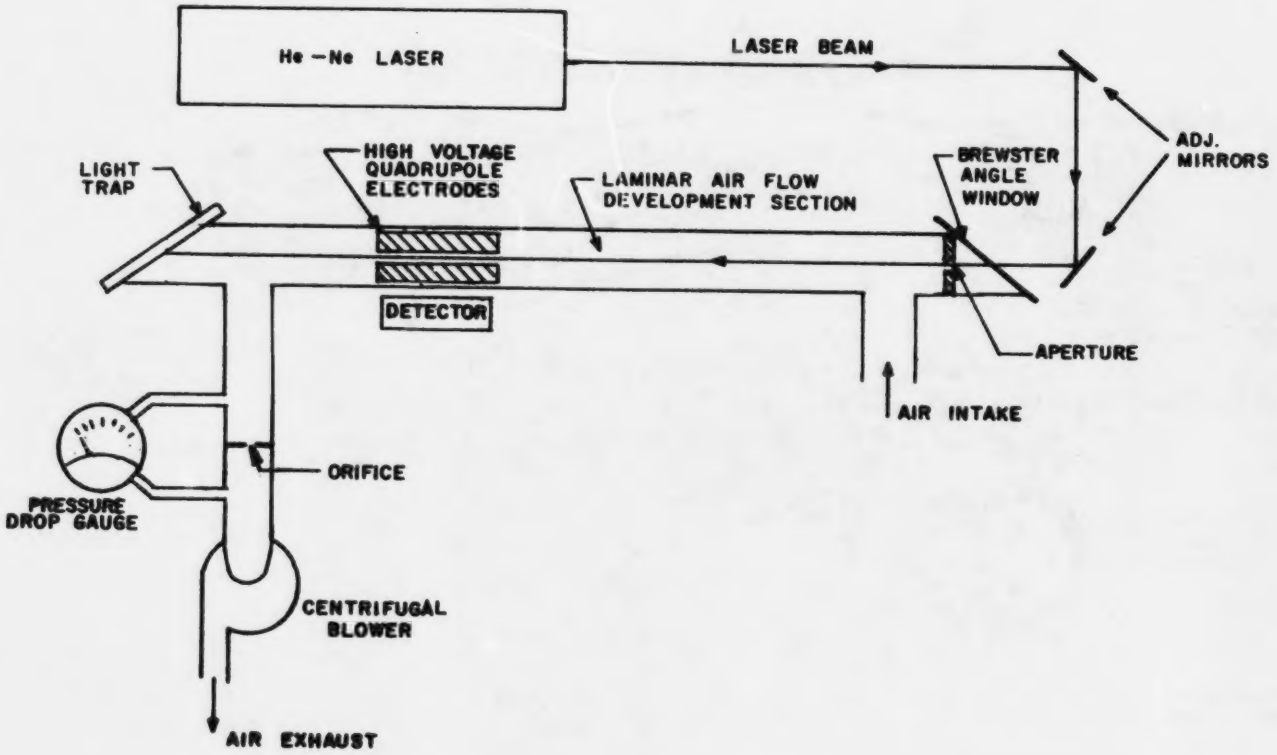

Figure 12. Schematic of optical and flow systems of FAM

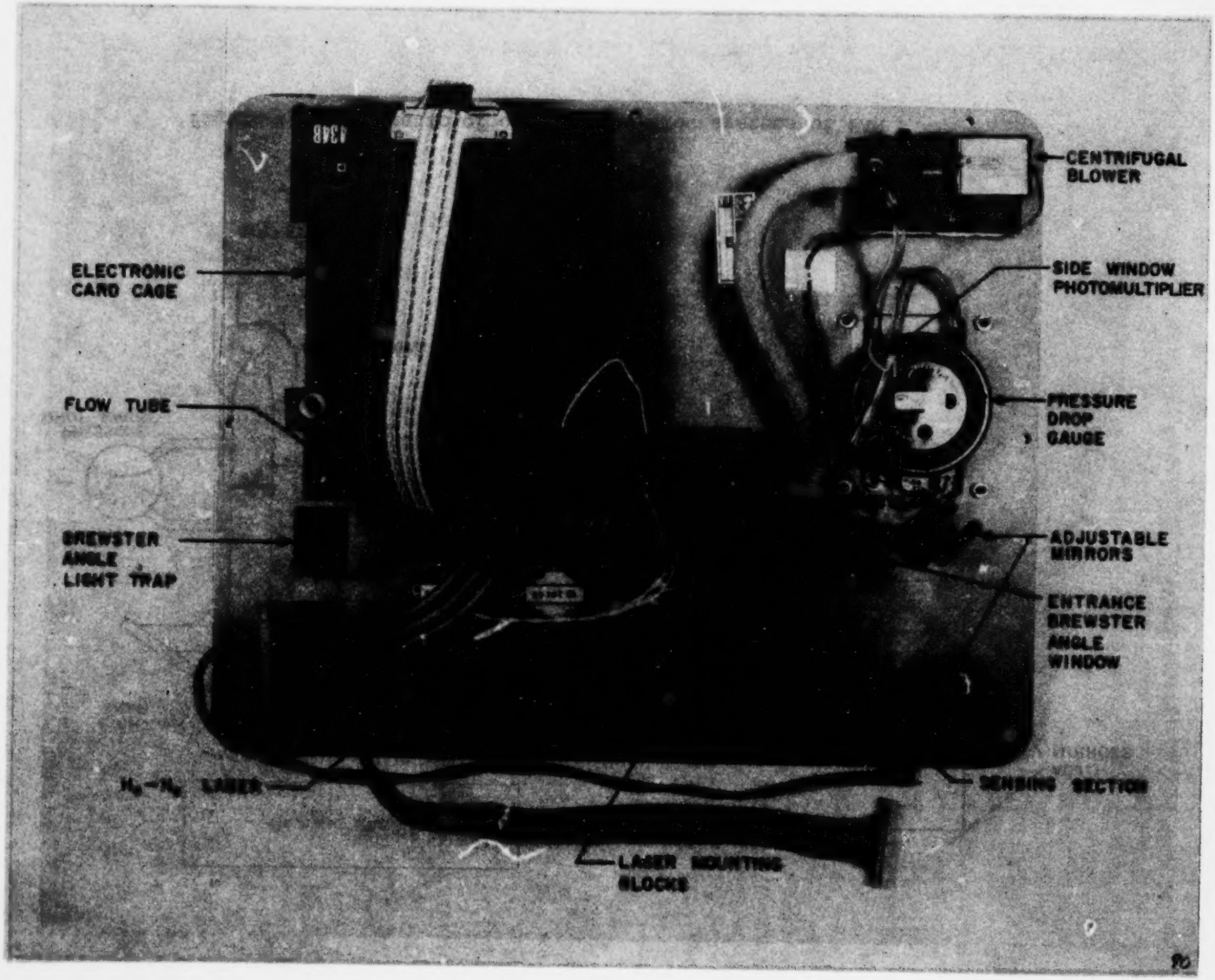

Figure 13. Optical and flow elements of the FAM

and their layout. This latter view is of the underside of the top panel of the instrument on which the optical and flow components, as well as the electronic card cage are mounted. This panel is made of an aluminum honeycomb sandwich with an overall thickness of 1 cm with the honeycomb enclosed between two aluminum sheets whose thickness is 0.5 mm each. The weight per unit area of this panel is 0.42 g/cm^2, or a total weight of about 0.7 kg which should be compared with a 4.5 kg aluminum jig plate with equivalent structural rigidity required for the optical system. The use of the honey-comb panel was dictated by the contractual overall instrument weight limitation of 13.6 kg (30 lbs), which would otherwise have been exceeded had a solid plate been used.

The helium-neon laser selected for the FAM was a Hughes* model 3222H-P laser with a larger than 500:1 polarization, with a minimum CW output power of 2 mW at 632.8 nm in the TEM_{oo} mode, having a beam diameter of 0.63 mm ($1/e^2$) and divergence of 1.3 milliradians, and a weight of only about 0.2 kg.

This laser was attached to the panel by means of two mounting block-clamps with rubber lining, as shown in Figure 13.

The two 45° mirrors are kinematic-mounting orthogonal adjustment front surface mirrors which are used to fold the laser beam by 180° and to align the beam with optical axis of the flow-sensing tube thus permitting a rigid mounting of both the laser and the detection tube.

The optical elements of the flow-detection tube are the entrance Brewster-angle (56°) glass window, and the exit Brewster-angle (57°) Corning ultraviolet transmitting glass type 7-54 with a thickness of 3 mm which constitutes the light trap for the primary beam. Conventional light traps generally employ multiple reflections of the unwanted beam by partially absorbing surfaces; at each reflection the beam intensity is reduced but scattering from surface imperfections and contamination usually produces spurious background radiation. To minimize these effects the above-mentioned light trap was devised making use of the high degree of polarization of the laser beam. This trap was composed of a single glass filter placed at its Brewster-angle to minimize reflection. Virtually complete light absorption is achieved by selecting the above-mentioned material whose transmission at 632.8 nm is negligible.

The light scattering photomultiplier tube detector used on the FAM is a 9-stage side-on type with a multialkali photocathode with a relative responsivity of about 26 percent, a quantum efficiency of about 2.2 percent and an absolute responsivity of about 5×10^5 A/W at the He-Ne wavelength of 632.8 nm. This photomultiplier (RCA type 4840) is packaged within an integrated assembly which includes a 12 volt d.c. to-high voltage converter, regulation circuit, dynode voltage divider network and an electrostatic/magnetic shield. This photomultiplier assembly is attached to the flow-sensing duct as shown in Figure 13. A 0.8 mm longitudinal slit within that mounting limits the angular scattering dispersion to about 1.5° in order to provide the necessary angular selectivity required to preserve the fiber scattering pulse sharpness information. The detection volume is viewed by the detector through the gap between two adjacent

---

*Hughes Aircraft Co., Industrial Products Div., Carlsbad, California.

electrodes of the rotating field quadrupole. These electrodes are thin copper foils cemented to the inside of a length of Pyrex tubing which serves both as an insulating support for the quadrupole as well as a transparent element for the scattered light in its path to the detector. All other optical support elements including the flow-sensing duct are made of black anodized aluminum.

Sampling-Flow System

The air flow system of the FAM is depicted in Figure 12. The air intake is a short section of vertical tubing with a diameter of 1.27 cm equal to that of the flow-sensing tube which forms a 90^{o} angle with the inlet duct. A 20 cm long laminar flow development section follows that bend, followed in turn by the sensing section whose inner diameter matches the rest of the tube in order to prevent any flow discontinuities. The length of this Pyrex section is 6.5 cm of which 2.5 cm constitutes the detection length. An additional 4.5 cm from the end of detection region is allowed to preserve flow straightness before the exit 90^{o} bend leading into the centrifugal blower through a flow constriction across which a pressure drop gauge (Dwyer Minihelic 0 to 0.5 in. H_2O range) is connected to provide sampling flow rate indication. For the rated flow rate of 2 liters/min the indicated pressure drops were 300 newtons/m^2 (1.2 in. H_2O) and 450 newtons/m^2 (1.8 in. H_2O) for the two prototype instruments.

The air driver is a miniature centrifugal blower powered by a brushless d.c. motor (Brailsford* mod. TB1-1L, 5 to 18 volts operation). This blower is a low pressure head device of low power consumption (approximately 0.5 watts) compatible with the generation of a pulsation-free 2 liter/min flowrate through an essentially open duct system whose major flow resistance consists of the flow measuring orifice discussed above.

In addition to the sampling-flow system described above the FAM was provided with an optional, external accessory for insertion into its inlet, consisting of a vertical elutriator designed to provide an approximate 50 percent aerodynamic particle cut-off of 15 μm. Vertical elutriation is, as discussed in a preceding section of this report, the preferred method of inertial size selection of fibrous-shaped aerosols, and is compatible with the low pressure capabilities of the selected air driver.

With the 2 liter/min flow rate and an inner duct diameter of 1.27 cm (1/2 inch) the axial flow velocity at the sensing volume is about 52.6 cm/sec (based on a fully developed laminar flow parabolic profile) which combined with a sensing length of 2.54 cm results in a fiber residence time of about 48 milliseconds. The volume of the sensing region is difficult to establish accurately because the effective laser beam diameter at the detection region is not known exactly. It is estimated that this diameter is about 0.7 mm, on the basis of the manufacturer specified beam divergence and on the geometry of the system. It should be understood that the effective beam diameter refers to that dimension within which fibers receive sufficient illumination to exceed the overall noise level associated with the entire beam width. The actual effective sampling flow rate is thus estimated at about 10 cm^3/min with respect to the total flow rate of 2 liters/min passing through the duct.

---

*Brailsford & Co., Rye, New York.

The flow-detection configuration of the FAM, wherein the illuminating beam diameter is a small fraction of the flow duct diameter was based on two principal reasons: (a) the need for a uniform flow velocity, within a laminar regime, within the illumination region precluding radially variable residence times, and (b) the requirement of a nearly uniform electric field where the sensing diameter is small with respect to the interelectrode spacing.

The sensing volume is, based on the above considerations, about 10^{-2} cm^3, which when replaced in equation (25) indicates a 1.6 percent coincidence probability for the simultaneous presence of 2 fibers within the detection volume for a fiber concentration of 20 cm^{-3}.

Quadrupole Electric Field Generator

The rotating field at the sensing region of the FAM is generated by two sinusoidal voltages, 90°-phase shifted with respect to each other and applied to each of the opposing electrode pairs of the quadrupole. The two sine voltages are generated by the circuitry shown on the schematic of Figure 14, and the high-voltage transformers of the schematic of Figure 15 (upper right corner). Referring to Figure 14, a quadrupole oscillator generates two 90° phase-shifted 400 Hz sinewaves which are then fed into a class A/B power amplifier circuit with feedback. Each of the two sinewaves is amplified separately and the output of the power amplifiers are fed into the primaries of two separate high-voltage transformers (Figure 15) with 1:300 turn ratios with grounded secondary center taps to insure proper potential balance at the quadrupole. The output voltage of each of the two transformers which is applied to the quadrupole electrodes is about 3000 V peak (6000 V peak to peak) which results in a nearly constant axial field intensity of 3000 V/cm (based on equation (13)). The power amplifier is required to provide the necessary primary drive to overcome the transformer losses along, since there is no significant output load except for the small capacitances and inductances associated with the high voltage leads and the quadrupole electrodes themselves.

The selection of the operating field parameters of 3000 V and 400 Hz for the rotating field generator were based on several considerations which will now be discussed.

It was concluded from the initial phases of the program that higher field intensities were to be preferred because of the improved definition in the resulting fiber orientation. It was determined both theoretically and experimentally that fiber jitter as a result of Brownian bombardment decreases with increasing electric field intensity. In addition it was considered that more intense fields would facilitate rapid fiber charge separation and the concurrent generation of the required dipole moment. Practical limitations imposed by the experimental transformers used on the FAM established an upper operating limit of 3000 V both from the power drive requirements as well as from the insulation capabilities of these devices.

The frequency of 400 Hz was, as in the case of potential, a result of theoretical and practical considerations. Lower rotational frequencies can be more easily achieved because of the decreased viscous drag. Operation at higher frequencies, however, provides a better signal-to-noise ratio since that ratio follows approximately a 1/frequency characteristic. The 400 Hz value was

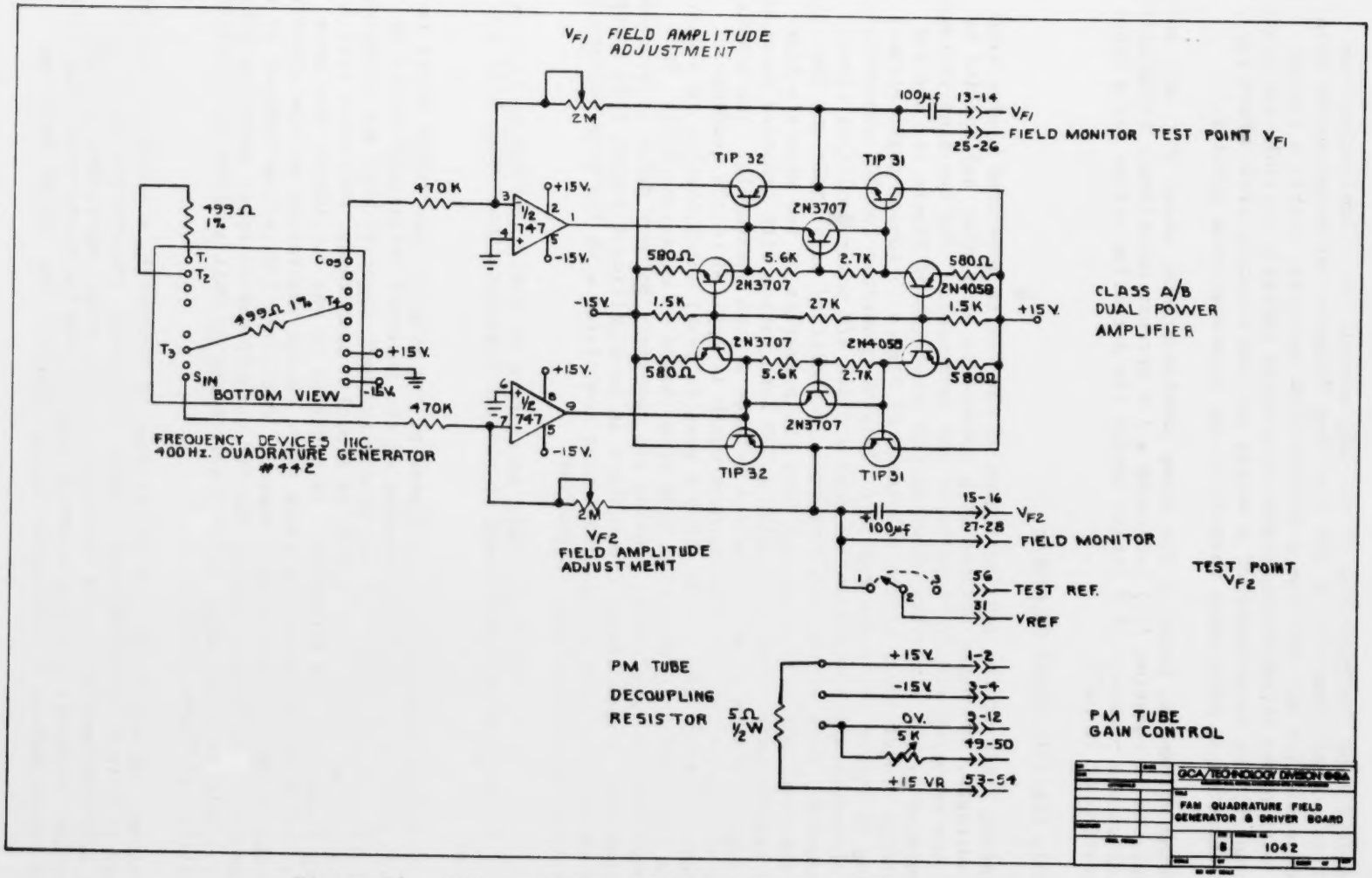

Figure 14. FAM quadrature field generator and driver board

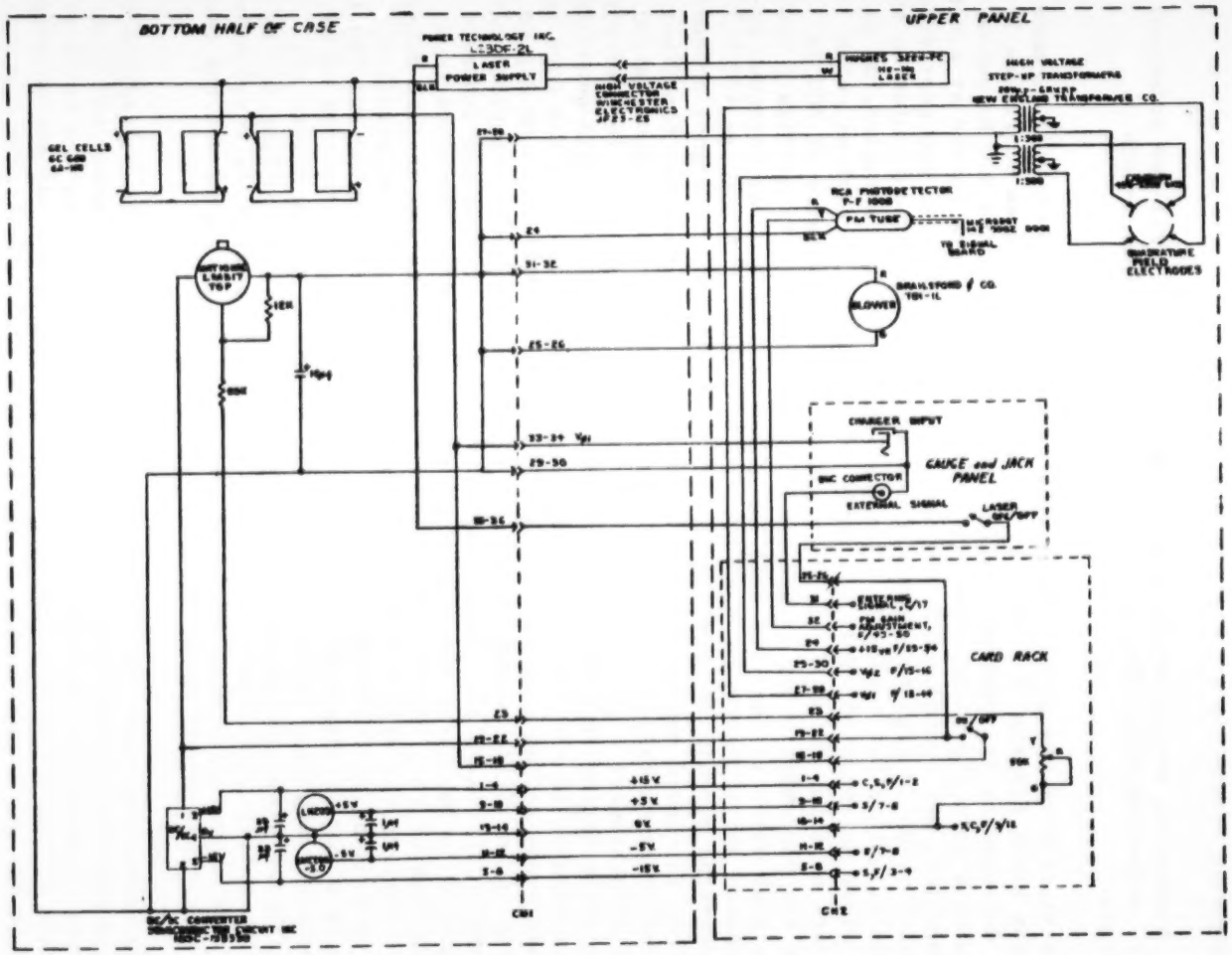

Figure 15. FAM overall wiring layout (note: the two capacitors across the ±15 V supply are 3.3 µf not 33 µf)

arrived at as a compromise between these conflicting effects as well as based on the frequency limitations imposed by the particular transformer design.

Signal Processing System

The signal processing system of the FAM was designed to fulfill two principal objectives: selective detection of discrete fibers and fiber length discrimination.

For the description of the signal processing circuitry reference will be made to the system block diagram of Figure 16 and the circuit diagram of Figure 17. The signal detected by the photomultiplier consists of discrete 800 Hz pulse trains resulting from the fiber rotation. Although the fibers rotate at a rate of 400 revolutions per second, each complete rotation results in two scattering pulses each of which is produced as the fiber axis becomes perpendicular to the detection axis. Since the residence time, within the detection region, of an individual fiber is about 48 msec, as mentioned previously, a typical pulse train consists of about 38 to 40 discrete pulses at the frequency of 800 Hz. The output from the photomultiplier is preamplified and buffered to provide a low impedance signal which is then fed into two phase-sensitive or synchronous detection circuits whose theory has been treated by a number of authors.[36-41] A signal inversion circuit is provided in order to subtract the signal present when the fiber is viewed end-on from the signal pulse obtained when the fiber axis is viewed side on (signal peak). This subtraction provides cancellation of unwanted asynchronous signals such as d.c. shifts, noise, etc. The reference signals for these gating controls are derived from the electric field generator circuit (see Figures 16 and 17). The primary gated signal is then fed into two similar synchronous gating channels labeled PSD No. 1 and PSD No. 2 on Figure 16 corresponding to the "side signal" and "central signal" channels, respectively of the schematic of Figure 17. These two gated channels provide two separate outputs required to implement the pulsewidth detection method described in a preceding section of this report. The electronic implementation of this method consists of sampling the signal contained within two fiber angular position ranges, corresponding to the central portion of the scattering pulse and the two symmetric side wings of this pulse, and integrating the signal over the 40 or so pulses associated with each passing fiber. The reference gating pulses are generated with the basic 400 Hz reference signal by frequency doubling and by generating two pulses of different width centered on the peak of detected signal and subtracting these two square pulses to obtain the central gate and the two side gates (see lines CG and SG of Figure 17).

It should be understood that the peak of the detected signal, for negligible viscous friction-associated phase lag, occurs at a phase angle of about 45° with respect to the peaks of the two high-voltage sinewaves applied to the field quadrupole. This 45° angle results from the fact that the optical detection axis passes between the gap formed by two of the adjacent field electrodes.

The output from the two synchronous detection amplifier stages representing the central and side parts of the detected pulses, after low-pass filtering, are then fed into integrator circuits to provide a broad signal pulse with a duration comparable with the fiber residence time. These two signals (i.e., representing the central and side parts of the original pulse trains) are then fed

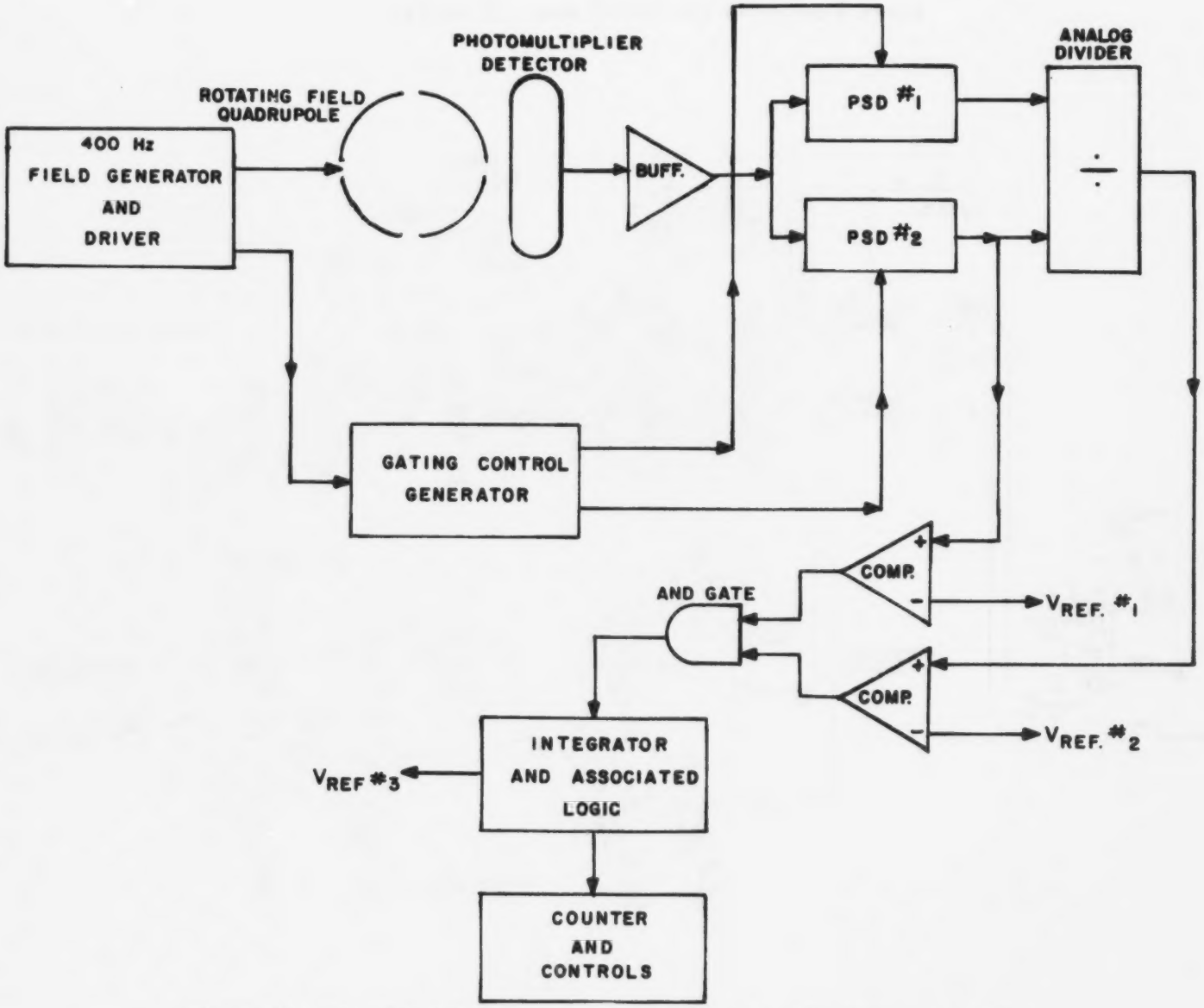

Figure 16. Overall block diagram of electronic subsystem of the FAM

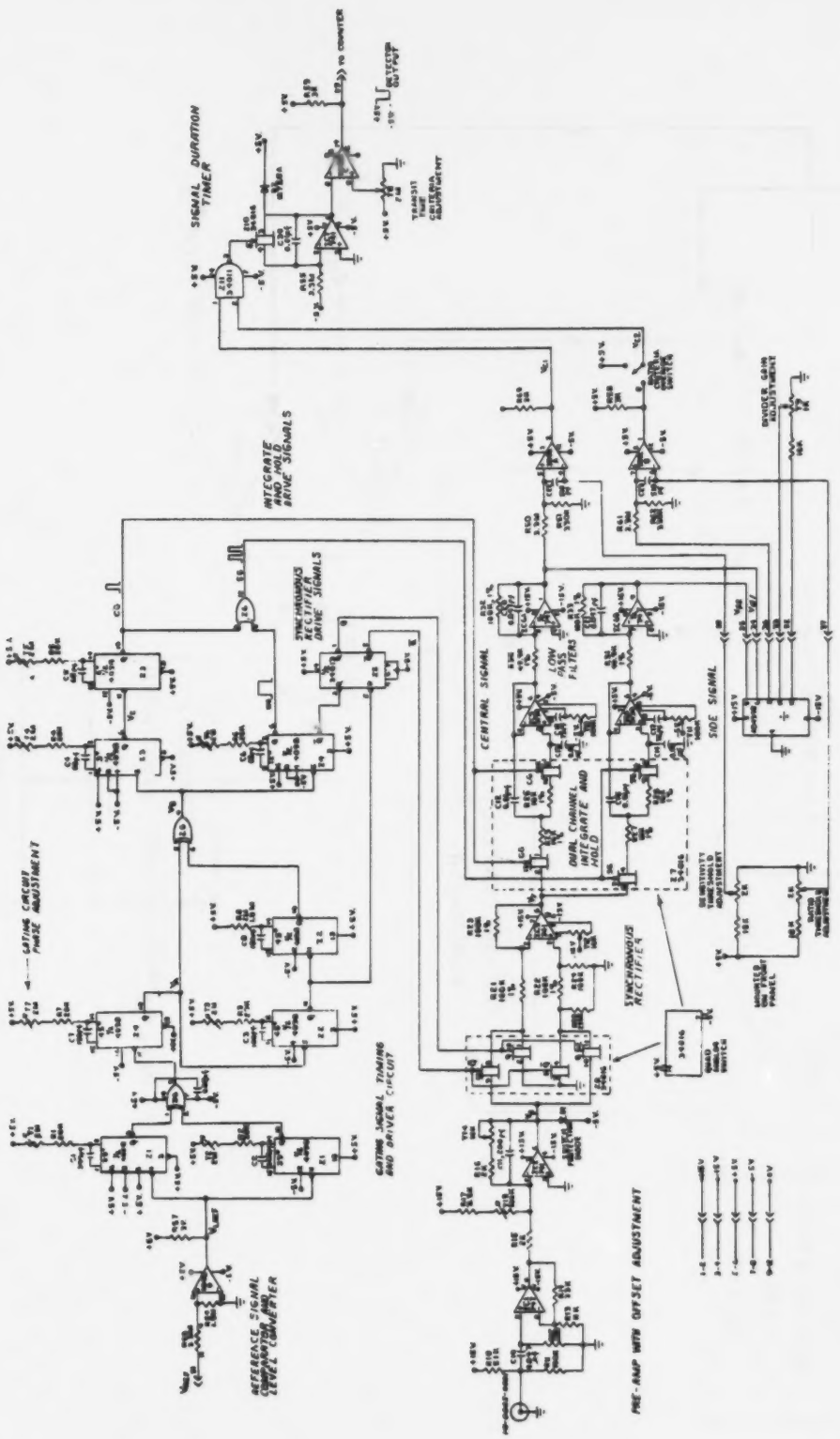

Figure 17. FAM gating and processing board

into an analog division or ratio module whose output is proportional to the ratio of the central pulse signal to the pulse wing contribution; i.e., an output signal related to fiber length as defined by equation (22). This ratio signal is entered into a comparator whose reference voltage can be adjusted on the instrument panel to select signals exceeding a selected level to be correlated with fiber length.

The output signal from the central part of the pulse signal is also fed into another comparator in order to accept only signals whose amplitude exceeds a selected minimum. This selection is performed to protect against low signal or noise associated ambiguities of the ratio operation. The two comparator outputs are connected to an AND gate which provides an output pulse only if both of the above-stipulated signal conditions are met; i.e., ratio and amplitude above predetermined values.

The resulting pulse is then integrated to perform a time-dependent selection; i.e., only signals that persist for a period comparable to the fiber residence time will be processed. A third adjustable comparator performs this last signal selection.

A ratio criterion override selector has been incorporated on the plug-in board such that for irregularly shaped fibers the ratio criterion can be bypassed leaving only the amplitude discrimination as a basis for fiber acceptance. The output from the last comparator (see Figure 17) consists of negative-going square pulses, one for each fiber, with a pulsewidth of the order of 25 msec.

The above described circuitry actually applies four different acceptance tests to every detected signal and only if all of these criteria are met is that signal train registered as a fiber count: (a) the signal pulses must be synchronous in frequency and phase with the internal reference waveform, (b) the average amplitude of the pulses of a train must exceed a preset minimum, (c) the average ratio of the central to the side portions of the pulses must exceed a preset minimum, and (d) the duration of the pulse train must exceed a preset minimum.

Counting-Display Circuitry

The output pulses from the time duration comparator, representing discrete fibers, are then fed into the counter and display circuit. The schematic of this section is shown in Figure 18. This circuitry consists of a 8.738 kHz oscillator followed by a $2^{(19)}$ frequency divider to provide a basic 1-minute counting gate. The display, a liquid-crystal readout, is driven by a 32 Hz waveform. When power is applied the unit automatically resets itself and displays one zero to the left and all zeros to the right of the decimal point. The decimal point position is controlled by the position of the count time selector switch and leading zeros are suppressed. Counting periods of 1, 10, 100 and 1000 minutes are selectable by the panel mounted switch. The display provides counts of up to 199,999 fibers. When the "start" button is pushed and released the counter initiates the counting operation with dynamic display. A "C" in the left-most digit position indicates it is in the counting mode and the decimal point is blanked out. At the completion of the counting period the unit stops counting input pulses, the "C" disappears and the decimal point appears in the proper

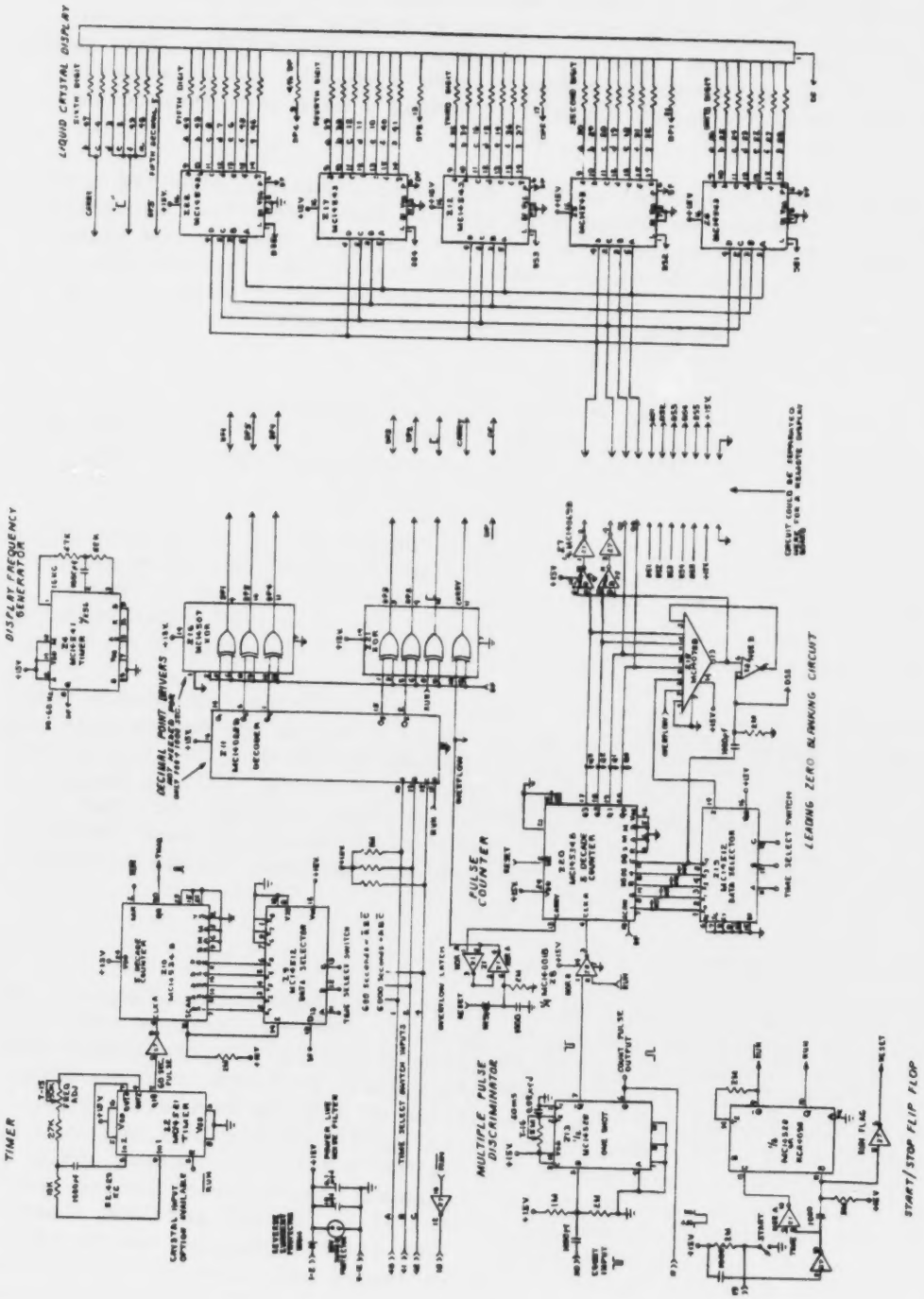

Figure 18. FAM counter and display boards

position, providing a readout directly in fibers/cm^3. The volume of air passing through the sensing region for a 1-minute sample is equal to about 10 cm^3/min, thus by displaying the fiber count accumulated over 1 minute and by automatic division by 10 the display indicates directly the concentration in fibers/cm^3. Thus, for the 1-minute count period the display resolution is 0.1 fibers/cm^3, for the 10-minute period it is 0.01 cm^{-3}, for 100 minutes it is 0.001 cm^{-3} and for 1000 minutes it becomes 0.0001 cm^{-3}.

Power Supplies and Power Consumption

The basic power source for the FAM is a set of four rechargeable gelled electrolyte batteries Globe* type GC660 connected in a series-parallel combination to provide a nominal output of 12 volts with a total capacity of 12 ampere-hours. This type of battery is very reliable, relatively inexpensive and can be subjected to numerous charge-discharge cycles without noticeable degradation (up to 1000 cycles can be expected if the battery is not allowed to discharge completely during each cycle). These batteries are completely sealed and can be operated in any position. Their charge loss under no-load conditions is of the order of 2 to 3 percent per month at room temperature. Extended storage at discharged conditions does not result in either cell reversal or loss of ability to accept recharge.

A Globe charger type GR6 122-000 CDM-12 volts was supplied as a separate item with each of the two prototype FAM's. This charger provides a variable current depending on the charge condition of the batteries. When operating the FAM the charger provides almost the entire replacement current to the system permitting nearly indefinite operation from the 115 volt a.c. line.

The nominal 12 volts from the batteries (in practice about 13.5 volts for a fully-charged condition) is supplied to the following elements of the FAM (see Figure 15): the laser power supply, a d.c.-to-d.c. converter with a high voltage output required for the operation of the 2 mW He-Ne laser; a d.c.-to-d.c. low voltage converter with an output of $\pm$ 15 volts for the operation of all the electronic circuitry, the input power to the photomultiplier assembly, and for the generation of lower voltages such as $\pm$ 5 volts for various circuit modules, and an adjustable voltage for the blower motor. All power supplies were selected on the basis of maximum operating efficiency in order to minimize the battery energy requirements. The contractual objectives called for a continuous battery operation of at least 4 hours between charges. This objective was met and somewhat exceeded as can be concluded from Figure 19 which indicates that the FAM operated continuously for 5 hours with its initial battery charge, during which the voltage dropped from about 13.3 V to 10.8 volts.

The power requirements of the various elements of the FAM prototype including the intermediate power required by the voltage converters are tabulated below. The total current drawn from the batteries averages about 2.8 amperes, which over a 4-hour operating period corresponds to a capacity of 11.2 ampere-hours or an energy of 480,000 joules (134 watt-hours).

*Globe Battery, Milwaukee, Wisconsin.

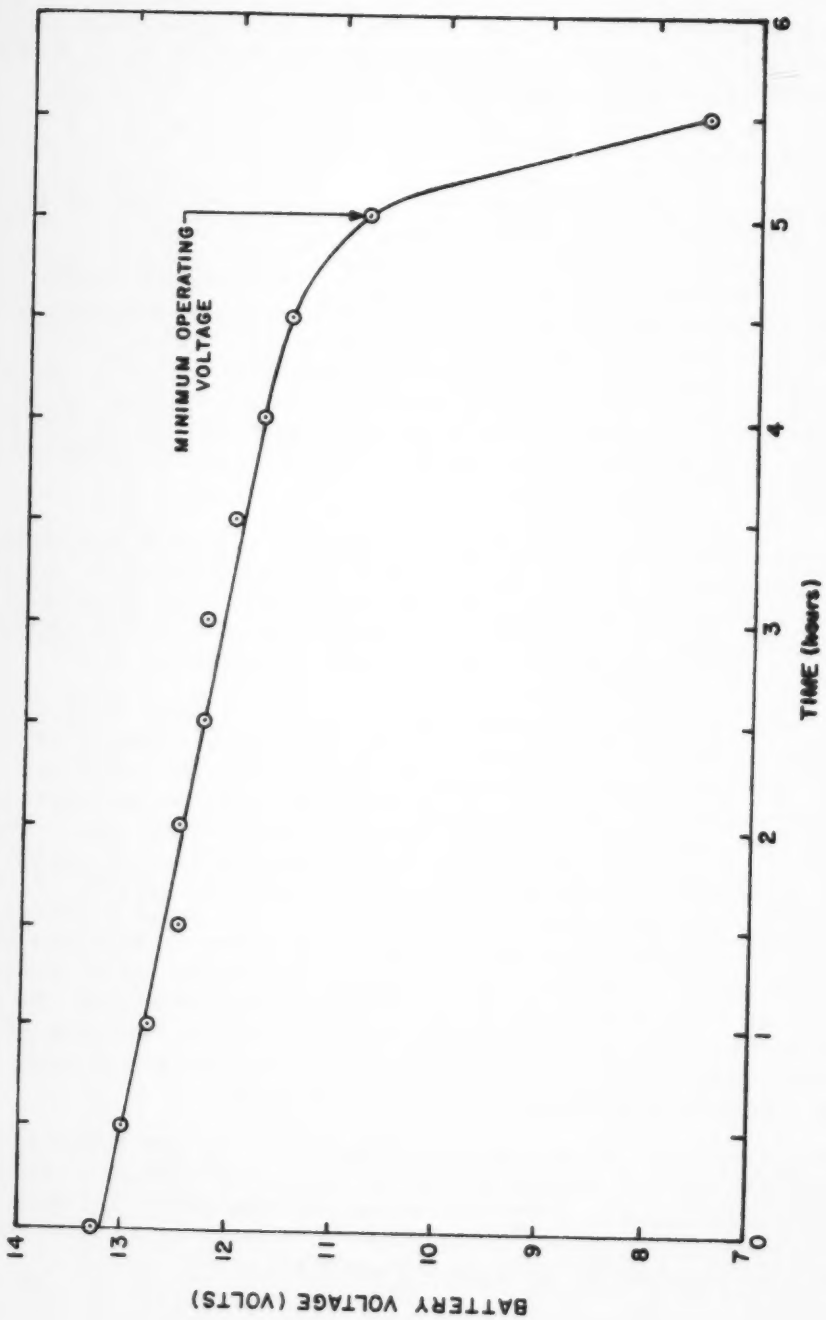

Figure 19. Battery output voltage as a function of FAM operating time

Table

He-Ne laser and d.c. to d.c. power supply combination	24.0 watts
Photomultiplier-power supply assembly	1.5 watts
Blower	0.25 watts
Electronic circuitry	7.75 watts
Total power	33.5 watts

Instrument Packaging Aspects

The contractual stipulations imposed the following limits on the overall instrument: (a) maximum weight without the charger but including the batteries of 13.6 kg (30 lbs), and (b) maximum volume, excluding charger of 56,600 cm^3 (56.6 liters or 2 cubic feet). The first of these two stipulations imposed stringent design constraints since one of the major weight contributors; i.e., the batteries (4.8 kg), could not be reduced given the power requirements and operating time specifications. The most significant weight reduction was achieved through the use of the honeycomb panel discussed in more detail in another section of this report. The final weight of the FAM (excluding the 1.5 kg cover) was about 13.5 kg.

The volume of the instrument without the separable cover was 26,000 cm^3, and with the cover 43,000 cm^3, both well within the maximum objective. The outside dimension of the enclosure are: 53.3 cm in length, 43 cm in depth and 11.4 cm in height for the basic instrument and 19 cm in height with the cover.

As can be seen in Figure 13 all optical and flow elements, the electronic circuitry card cage assembly, the controls and display, the blower and flow readout are mounted under the top honeycomb panel, which can be separated from the rest of the instrument as an integrated assembly. The batteries, laser supply, and the low voltage supply are mounted directly to the bottom of the metal enclosure, a drawn aluminum case. The top panel is mounted on this enclosure with a foam rubber gasket to prevent access of dust into the interior of the FAM (see Figure 20). The card cage for the electronic circuitry contains three plug-in cards with wire-wrap wiring. The entire card cage can be lifted up into a locked position above the panel for easy access to the electronic circuitry, as shown in Figure 21.

PROTOTYPE AEROSOL TESTING

Aerosol tests of the FAM both during the developmental stages as well as during the final evaluation of the deliverable prototype instruments consisted mainly of a series of fiber count comparisons between the FAM output information and optical microscope counts of filter collections of the aerosol downstream of the instrument. Microscopy was performed following the NIOSH phase contrast method as discussed in a preceding section of this document. The test were performed by introducing the aerosol, as generated by the device of Figure 11, into the inlet of the FAM using as much dilution air as required to establish a 2 liter/min flowrate. For these tests an external pump was used placing the reference filter directly downstream of the FAM and bypassing the internal blower

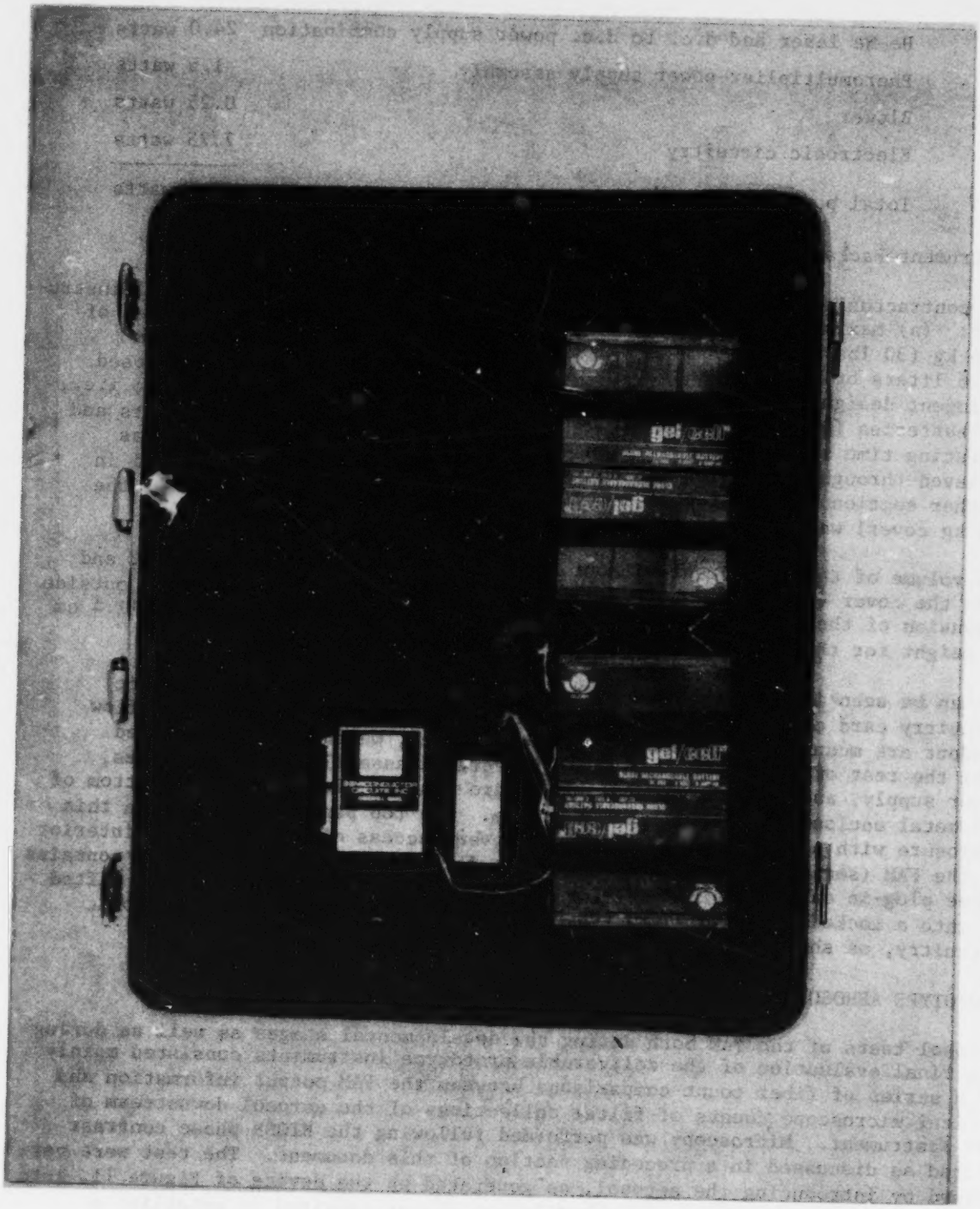

Figure 20. View of bottom of FAM enclosure with panel removed

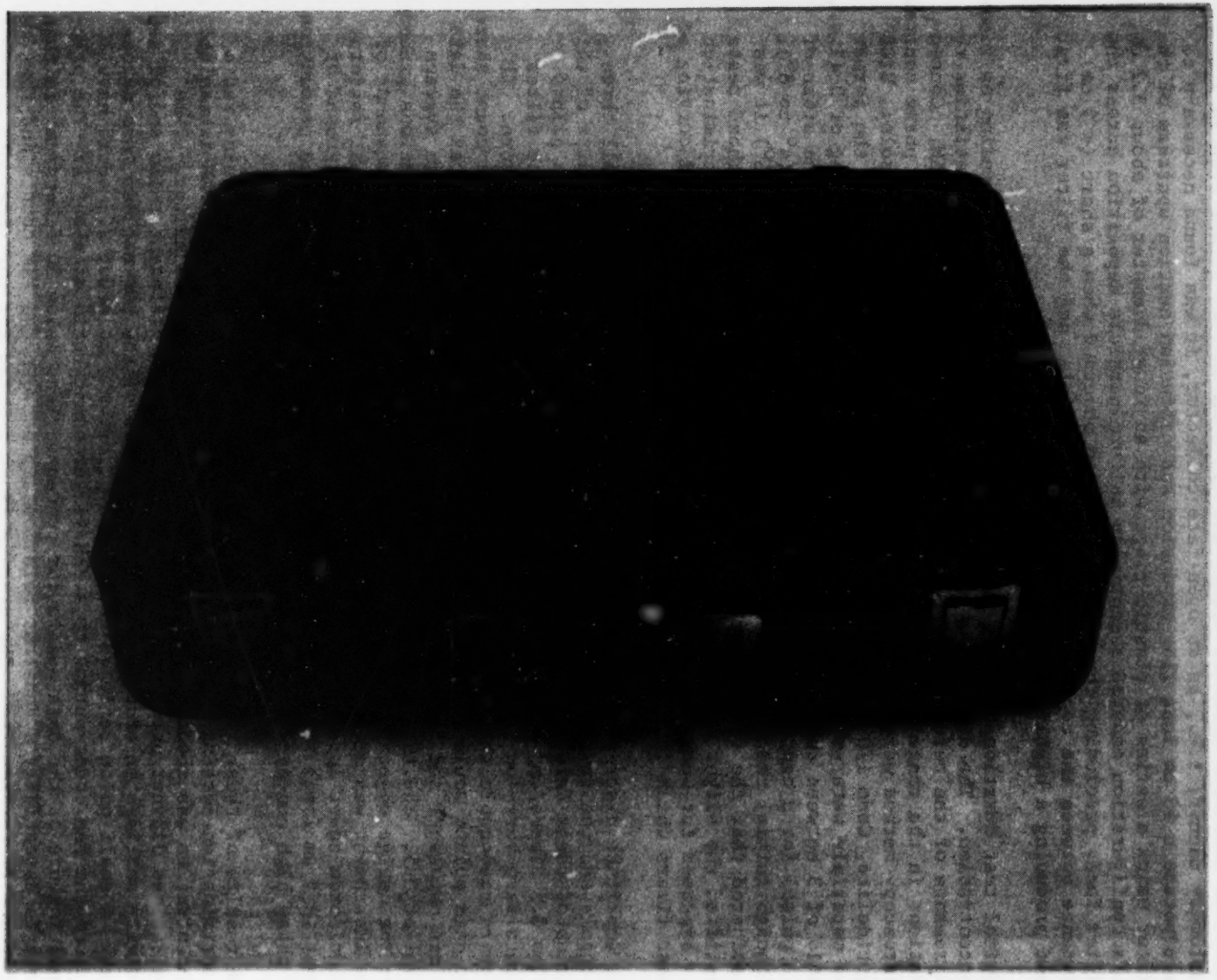

Figure 21. Top view of FAM with electronic circuitry card cage in the lifted-up position

in order to prevent errors associated with fiber losses within that air driver. Since the reference membrane filter was operated in line rather than in its customary manner; i.e., as an open face collector, it was found necessary to incorporate a 13 cm long flow expansion and diffusion section upstream of the filter using a series of plastic rings with an inner diameter of about 3.2 cm. This configuration ensured essentially uniform particle deposition across the filter face, precluding the direct impaction observed when a short (< 2 cm) distance between the constricted filter holder inlet and the filter was first used producing a highly nonuniform deposition.

Typical test durations were in the range of 10 to 100 minutes depending on fiber concentration. The duration of the tests was based on counting statistics requirements of the reference filter collection as well as for the FAM. Concentrations in the range of 0.4 to 40 fibers/cm^3 as determined by the phase contrast microscopy method were generated using three types of fibrous aerosols: UICC Crocidolite, Code 110 fiber glass and UICC Chrysotile. Tests with the former two materials were performed with the signal ratio threshold setting of 3 (i.e., ratio of 3 between the central part of the pulse with respect to the sides of the pulse) for a central gating width of $\pm 4^o$ and side gates of $\pm$ (4^o to 8^o). Although initial testing had been performed for $\pm 3^o$ and $\pm$ (3^o to 6^o) it was considered that the finite degree of pulse jitter observed during those tests justified the slight widening of the gating widths. The ratio discrimination was bypassed for Chrysotile because of the extreme irregularity and curving of these fibers which invalidated the ratio sensing.

The amplitude discrimination was set to a dial reading of 0.5 for all three aerosols and the tests were performed as described above. The results of this series of these aerosol tests are shown in Figure 22. The two data points below 0.5 fibers/cm^3 are somewhat questionable because the reference filter counts were very low resulting in potentially large statistical errors. It appears reasonable that for a statistically more accurate reference count these two data points would have been close to the same FAM/filter ratio as the data points between 1 and 30 fibers/cm^3 which fell reasonably close to an average level of 0.5. The two data points above 30 mg/m^3 were at concentrations exceeding the design objective of the FAM; i.e., 20 fibers/cm^3, and the response of the instrument was obviously inadequate as a result of two concurrent factors, coincidence count losses and the presence of a large continuum background of short (< 5 μm long) fibers whose generation was concomitant with the production of these high concentrations.

The results of these tests can be interpreted as follows. For a pulse ratio discrimination setting of 3 and an amplitude setting of 0.5 the FAM-determined concentration was about 1/2 that indicated by the reference filter. Time limitations did not permit to rerun these tests with different ratio and/or sensitivity settings in order to bring the results of the two methods into agreement. A small pulse ratio adjustment; e.g., from 3 to about 2.5 would have shifted the FAM count output to a FAM/filter count ratio of about 1. The principal feature of the data points for concentrations below 30 fibers/cm^3 is that there is essentially a constant relationship between the FAM counts and the reference filter results. The precise final setting for the threshold controls must, of course, be obtained by a more extensive testing program and the above reported results are to be considered only as preliminary, although very supportive information on the performance of the FAM.

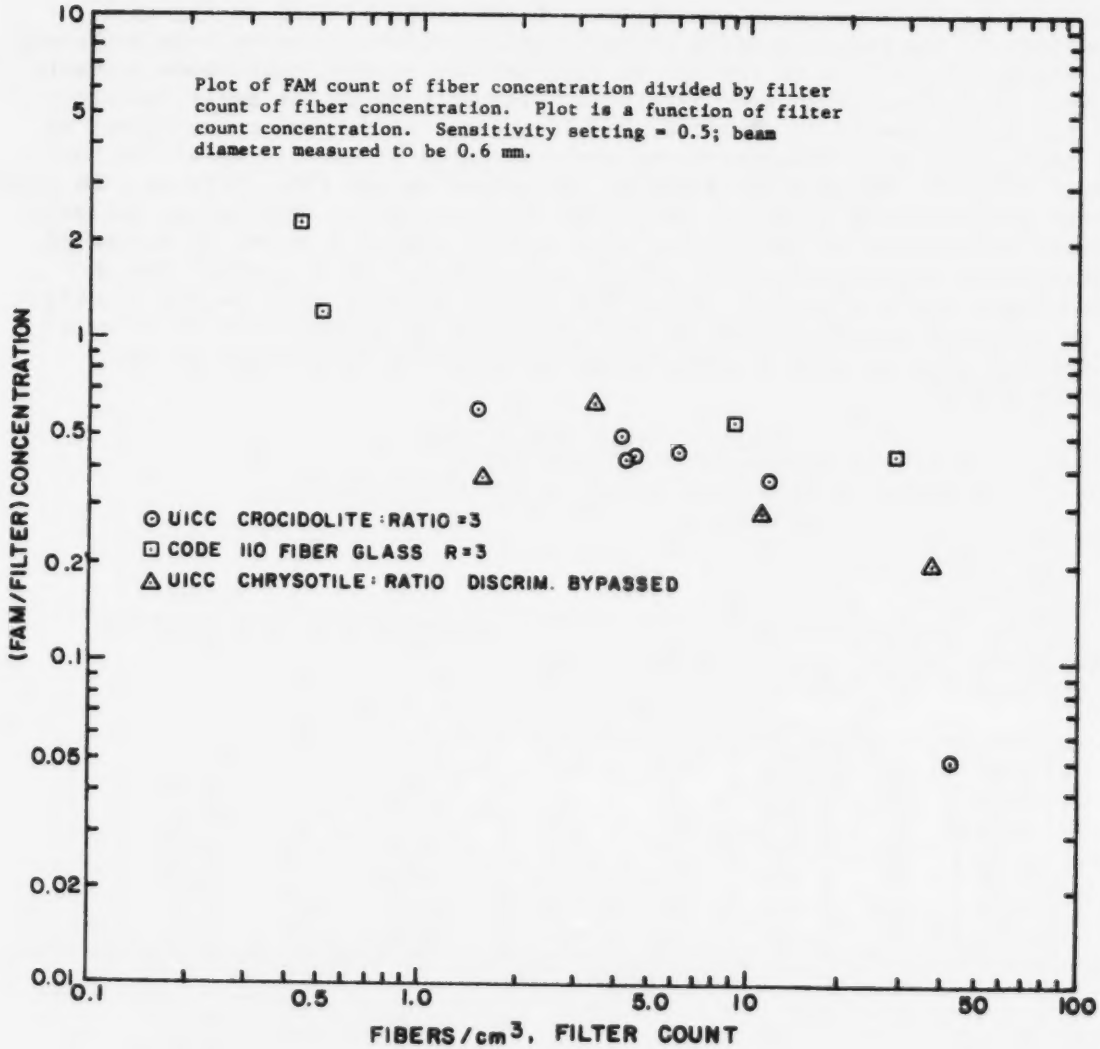

Figure 22. FAM test data

It should also be considered that the conversion of FAM counts over a given sampling period to fiber concentration involves a parameter whose exact value, although constant, is not known; i.e., the effective cross sectional area of the sensing volume, an uncertainty that has been discussed previously. Therefore the FAM count duration required to achieve the agreement between the reference method and the FAM results was only an approximation based on an estimate of the effective laser beam cross section at the sensing region.

Table 3 lists all the relevant parameters of the tests plotted in Figure 22. In addition to the tests reported above several qualitative tests were performed to determine the ability of the FAM to discriminate against nonfibrous aerosols. Two types of such aerosols were generated, cigarette smoke for small, submicrometer particles, and 12 μm diameter plastic spheres to determine the effect of large particles. Mass concentrations were estimated at several mg/m^3 for both types of aerosol. Neither one produced any counts on the FAM. Arizona road dust, however, generated FAM counts at very high concentrations. Microscope analysis of filter collections of this latter type of dust showed a number of elongated particles with length-to-diameter ratios exceeding 2.5 or 3 to which the observed counts were attributed. These FAM counts, however, only became significant at very high concentrations of dust, possibly in excess of 10 or 20 mg/m^3 when uninterrupted streams of such elongated particles was present in the detection volume.

Table 3. Test data of FAM.

FAM and filter count versus concentration ratio 3, sensitivity 0.5 (75 mV), gate 8°

Run	Date	Duration (min)	FAM count	Filter count		FAM concentration (cm^{-3})	Filter concentration (cm^{-3})
				Fibers	Fields		
UICC crocidolite							
1	4/22	10	385	50	64	4.3	11.7
2	4/22	20	329	51	88	1.81	4.32
3	4/28	57	1076	159	10	2.1	41.8
4	4/28	40	770	76	68	2.1	4.19
5	4/28	32	812	101	76	2.84	6.22
6	4/29	60	884	95	53	1.65	4.5
7	4/29	63	485	50	83	0.9	1.4
Fiber glass code 110							
8	5/2	17	738	96	96	4.85	8.82
9	5/3	8	895	102	67	12.5	28.6
10	5/3	78	705	33	147	1.01	0.43
11	5/4	100	524	40	122	0.585	0.49
UICC chrysotile ratio discrimination bypassed							
12	5/9	15	960	112	31	7.07	36
13	5/16	35	676	48	60	2.16	3.43
14	5/17	85	407	50	55	0.53	1.59
15	5/18	35	961	65	25	3.06	11.1

PROTOTYPE INSTRUMENT INSTRUCTION MANUAL

SPECIFICATIONS

- Total fiber concentration range: 0.0001 to 20 fibers/cm^3
- Minimum detectable fiber length: 2 micrometer (estimated)
- Minimum detectable fiber diameter: 0.2 micrometer (estimated)
- Counting periods: 1, 10, 100, and 1000 minutes
- Concentration resolution: 0.1 cm^{-3} for 1 minute period
  0.01 cm^{-3} for 10 minute period
  0.001 cm^{-3} for 100 minute period
  0.0001 cm^{-3} for 1000 minute period
- Maximum count rate: 20 sec^{-1}
- Maximum total count: 199,999
- Display: 7 segment, 1.27 cm high, liquid crystal, 6 digit.
- Ratio threshold control range: 0 to 10
- Intensity threshold control range: 0 to 10 (0 to 500 mV)
- Output pulse signal: + 15 volts, 20 msec, 3.5 mA max. (1 TTL gate)
- Flow rate (nominal): 2 liters/minute (adjustable 1.5 to 2.5 liters/min)
- Light source: 2 mW He-Ne laser (λ = 632.8 nm).
- Minimum duration of continuous operation with initially fully charged batteries: 4 hours.
- Battery voltage (nominal): 12 volts
- Operating current (typical): 2.8 amps
- Weight (without cover): 13.5 kg (30 lbs)
- Weight (with cover): 15.2 kg (33.5 lbs)
- Dimensions: 53.3 cm length, 43 cm depth and 11.4 cm height (without cover), 19 cm height (with cover).

OPERATING PROCEDURES

Reference will be made to the photograph of Figure 23. The numbers in parenthesis refer to those called out on that figure.

Identification of Top Panel Component Placement

(1) ON-OFF power switch

(2) START-RESET pushbutton switch

(3) Sampling period selector

(4) Sensitivity threshold control

(5) Ratio threshold control

(6) Count-concentration display

(7) Pulse output connector

(8) Laser ON/OFF momentary pushbutton switch

(9) Battery charger receptacle.

(10) Flow inlet

(11) Flow exhaust

(12) Flow readout gauge

(13) Flow readout zero adjustment screw

(14) Flow rate adjustment control.

Start-Up and Measurement Procedure

Set controls (4) and (5) to 0.5 and 2.5 respectively, or to those settings that have been established by independent comparison measurements. An approximate 5 μm length discrimination is obtained with the above settings.

Check flow rate gauge zero reading. If necessary correct with screwdriver adjustment (13).

Place switch (1) in the ON position, this applies power to all elements of the FAM.

Select the desired sampling period with selector (3).

Allow about a 1-minute warm-up period before proceeding.

Observe flow rate gauge (12), its reading should be between 0.1 and 0.2 inches of water (340 to 680 newtons/m^2). The calibrated 2 liter/minute reading is marked on the rear of the instrument. If the appropriate flow reading is not indicated (after a maximum warm-up period of 10 minutes), adjust with a small screwdriver the flow rate to the correct value with control (14). Correct flowrate will only be obtained if there are no flow constrictions either at the inlet (10) or at the exhaust (11) ports.

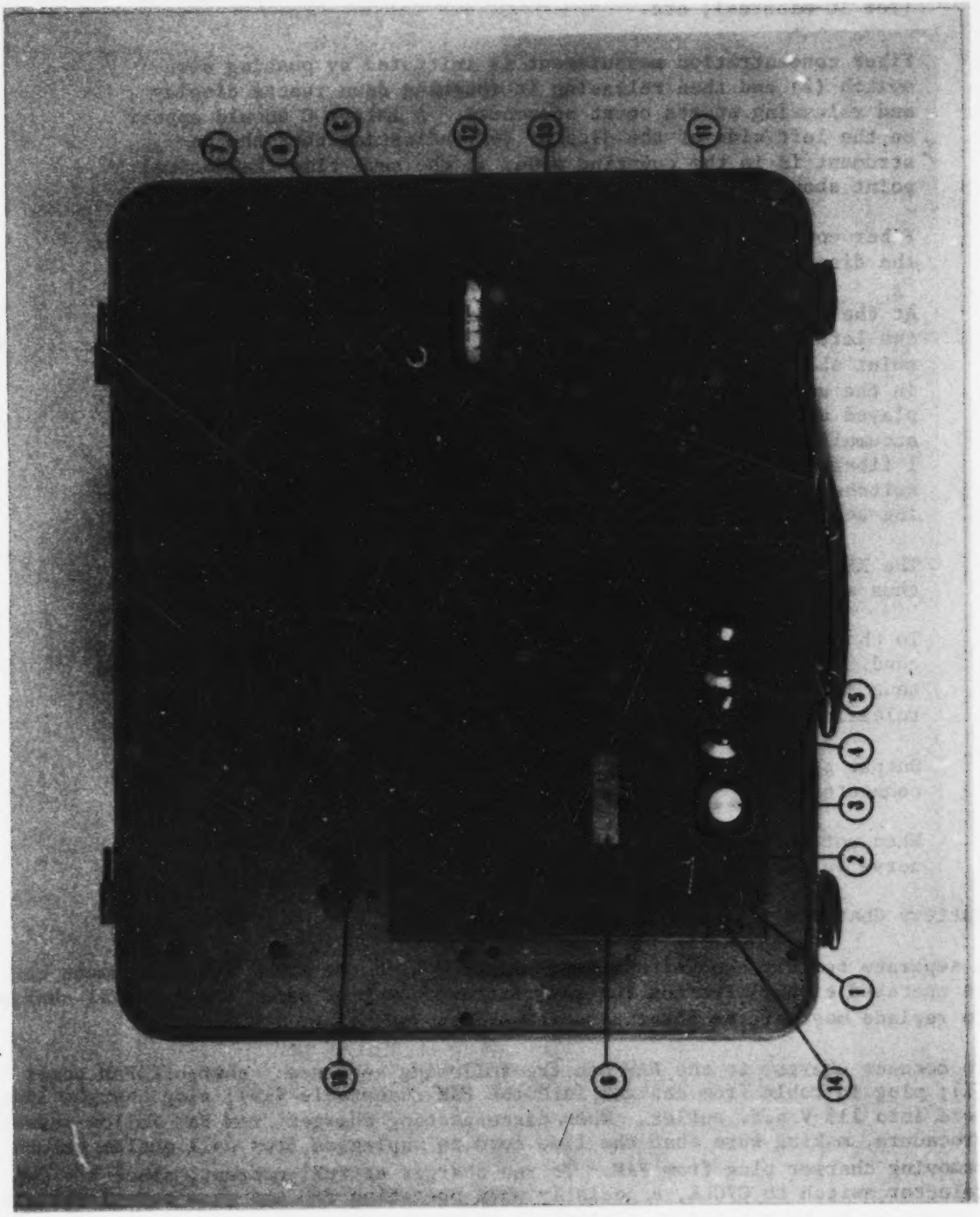

Figure 23. Top view of FAM

Observe digital display (6). Its readout should indicate 0.0 (for a 1-minute sampling time selector (3) position), 0.00 (for 10-minutes), etc.

Fiber concentration measurement is initiated by pushing down switch (2) and then releasing it (pushing down resets display and releasing starts count sequence). A letter C should appear on the left side of the display (6) indicating that the instrument is in the counting mode; at the same time the decimal point should not be displayed.

Fiber count is displayed dynamically; i.e., as a fiber is detected the display will increment by one count.

At the completion of the selected sampling time, the letter C on the left side of the display should disappear and the decimal point should reappear in the proper place to read out directly in the units of fibers/cm^3. The concentration value remains displayed until either the FAM is shut off or it is reset. If the accumulated fiber count is consistently less than about 10 (e.g., 1 fiber/cm^3 for a 1-minute period) the sampling time should be switched to a longer period in order to achieve an adequate counting accuracy.

The RESET-START switch (2) can be operated during a count period, thus starting a new count sequence.

To check system noise, if necessary, or to determine battery charge condition, the laser power push button switch (8) can be depressed thus shutting off the laser; power to the laser is restored when releasing switch (8).

Output pulses for recording purposes are provided at the BNC-type connector (7). Each pulse corresponds to a single fiber.

When not counting fibers it is desirable to shut-off FAM to conserve battery power.

Battery Charging

A separate battery charger has been provided with the FAM. The instrument can be operated either with the internal battery power or using the external charger to replace most of the power required by the FAM.

To connect charger to the FAM use the following sequence: shut-off FAM power (1); plug in cable from charger into the FAM receptable (19); plug charger line cord into 115 V a.c. outlet. When disconnecting charger from FAM follow reverse procedure, making sure that the line cord is unplugged from wall outlet before removing charger plug from FAM. To run charger at full current, place its own selector switch to CYCLE, especially when operating FAM and when normal charging current is to be applied to batteries.

To maintain full charge over extended periods of time when not using the FAM, place the charger selector to FLOAT.

ELECTRONIC TESTING AND ADJUSTMENT PROCEDURES

Signal Detection Circuitry

Reference is made to Figures 17 and 24.

1. Ground the signal input located at the micro-connector on the Signal Board. A 800 Hz square wave will be present at V_γ, the output of the synchronous rectifier (pin 6 of IC3). Trim T_{13} until the p-p amplitude of this square wave equals zero volts.

2. A d.c. offset at $V\gamma$ may be present. This should be nulled by T_{12}.

3. Adjust T_{10} until V ϕ 1, available at pin 6 of the AD434B analog divider, equals -10 millivolts.

4. Adjust T_{11} until V ϕ 2, pin 9 of the analog divider, equals +10 millivolts.

5. Input a 100 mv p-p, 800 Hz, square wave and trim T_{14} until V_β = 1 volt p-p (IC2, pin 6).

6. Change the input to a periodic square burst signal with a 35 msec burst duration. The square burst frequency should be 800 Hz with a coherent, 400 Hz reference signal available. The reference signal should be input to pin 56 of the Field Board and the slide switch positioned as to conceal the white dot.

7. Set the ratio knobpot to 1.0 and adjust T_9 until a count just begins to register.

8. Reset the slide switch on the Field Board so it displays the white dot and ground the signal input. Adjust T_{13} until V_β = -4v.

Gating Circuitry

1. Adjust T_1 until the duration of the period pulse present at Z6 pin 1 equals 7 μ sec.

2. Repeat this procedure for T_2 available at Z6 pin 2.

3. Set the duration of the pulse at Z6 pin 5 to approximately 35^o (240 μ sec) by trimming T_7.

4. T_3 is used to adjust the duration of delay pulse, which multiplies the frequency of the gating function. It is important that this delay represents 90^o of the field frequency ($\frac{1}{400\ Hz} \times \frac{90^o}{360^o} = 625\ \mu$ sec).

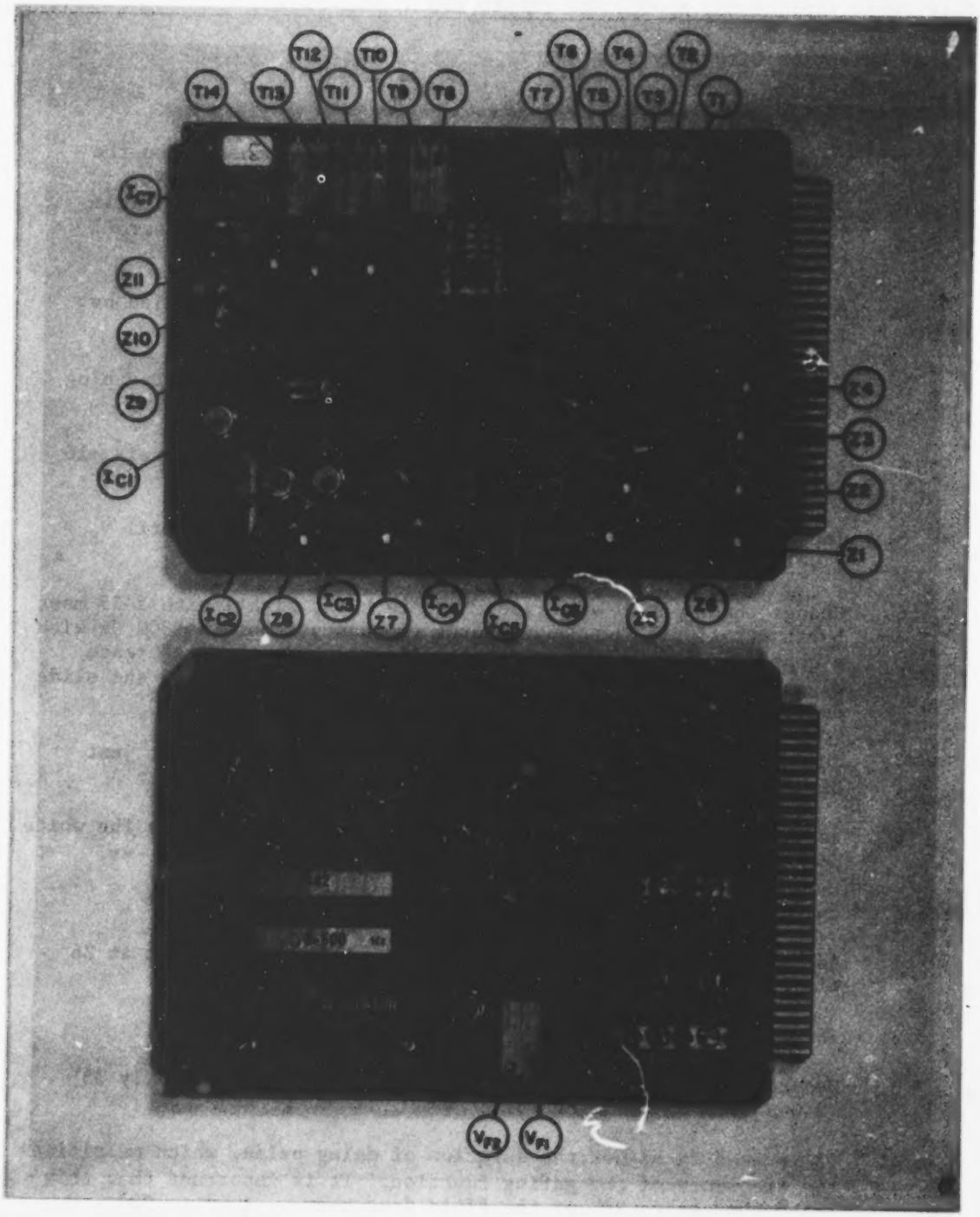

Figure 24. Top views of quadrature field generator-driver and of gating-processing boards

Adjust T_3 until the falling edge of this delay pulse, available at Z6 pin 4, meets this condition.

At this point the desired signal gating duration must be set. We will assume the center gate (CG) width to be 8^o (55.5 μ sec) making the side gate (SG) widths each 4^o (27.8 μ sec). If the desired sampling differs from 8^o the procedure remains the same; providing the appropriate symmetry is maintained.

5. T_5 directly sets the center gate duration. Adjust this for an 8^o pulse at Z6 pin 9.

6. Adjust T_6 to yield a 16^o (111 μ sec) wide gate (WG) duration (twice that of CG) available at Z6 pin 8.

7. The side gate (SG) sampling signal is formed by subtracting the center gate from the wide gate. The CG, located at Z6 pin 10, should be centered by T_4 yielding a symmetrical SG signal of two 4^o pulses.

The gating system alignment should now be complete. Final adjustment synchronizing the gate phase position with the actual signal phase must be performed when an actual signal is available from the fibrous sample. At that time T_7 should be used to make this adjustment.

Counter-Display Circuit

Reference is made to components on Figures 18 and 25.

1. The sampling period time base is adjusted by means of T15. This adjustment determines the sampling time time periods which have been adjusted to 1, 10, 100 and 1000 minutes. If it is found necessary to deviate from these values by a constant factor, T15 should be used.

2. The pulse period during which the counting circuit does not respond to any new fiber can be adjusted by means of T16, whose factory setting is for 20 msec pulsewidths.

OPTICAL ALIGNMENT PROCEDURE AND CLEANING

Refer to Figures 13 and 23.

1. Remove top FAM panel from case by removing the eight outermost screws (Figure 23).

2. Carefully place this panel upside-down on top of the case.

3. Rotate the laser about its axis to a position minimizing beam reflection from the Brewster angle window at the light input end of the aerosol duct assembly (ADA).

4. Remove the Brewster angle light trap.

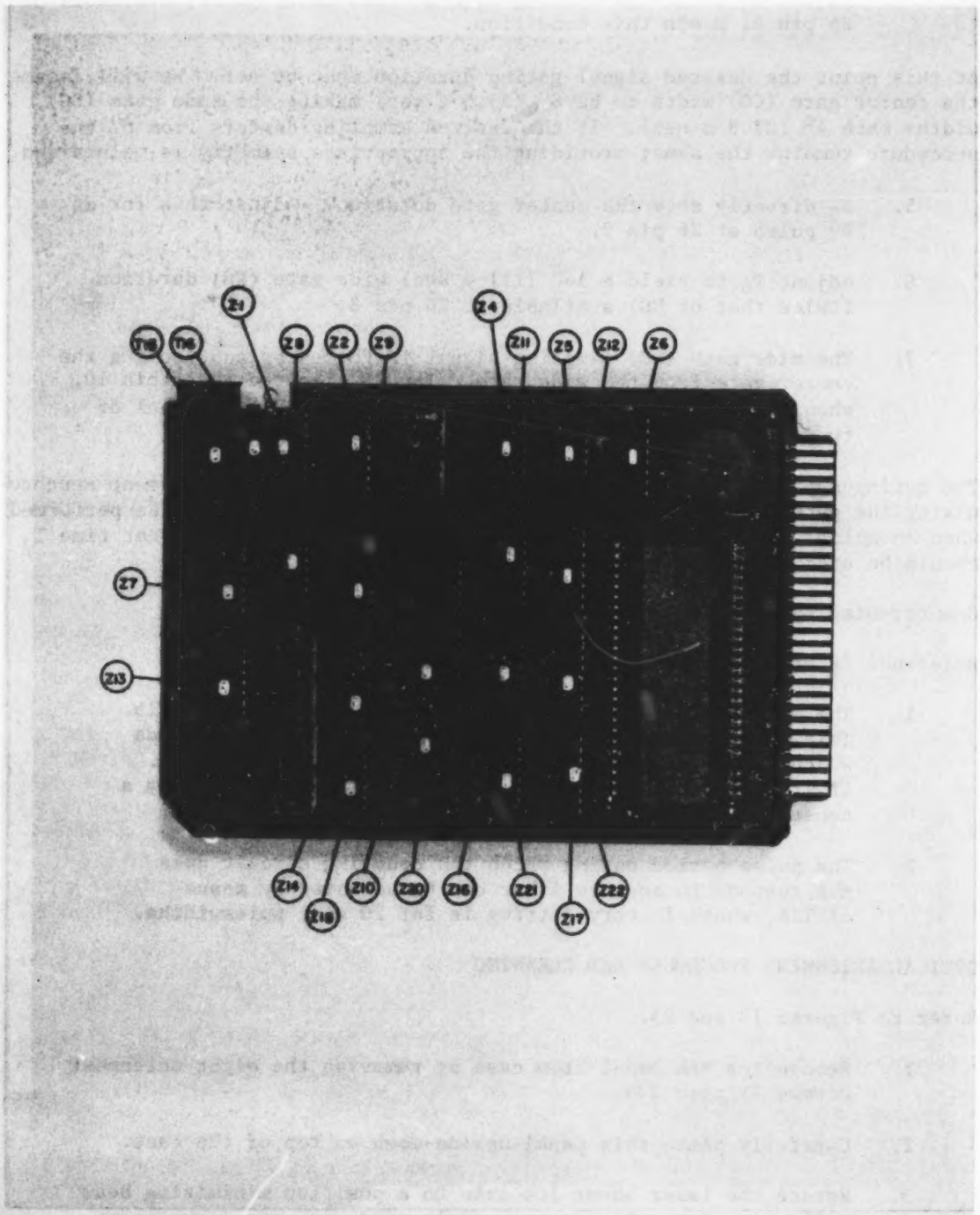

Figure 25. Top view of counter-display board

5. Carefully replace main panel on the carrying case and tighten the eight screws gently.

6. Remove both side access panels of carrying case.

7. Place FAM with panel facing down.

8. Insert alignment aperture, supplied with FAM, about 1 cm into beam exit end of ADA.

9. Place power switch (1) to ON. CAUTION: do not look into the laser directly at any time.

10. Adjust the mirror closest to the laser until the beam goes through the center of the entrance aperture.

11. Adjust the other mirror closest to the flow tube until the beam goes through the center of the exit (alignment) aperture by observing the laser beam spot reflected by a dark surface. Repeat steps 7 and 8 until beam is aligned with both apertures.

12. Remove alignment aperture and replace Brewster angle light trap. Be sure both O-rings are properly in place.

13. Replace side access panels.

NOTE: If main panel hold-down screws are loosened or tightened realignment may be necessary.

The access of coarse dust or dirt to the FAM inlet should be prevented as this material would tend to deposit on the window and light trap internal surfaces. Occasional cleaning of the interior of the flow-sensing duct should be performed, especially if coarse dust contamination is suspected, by removing the end windows as described in steps 6, 7 and 13 of the above described alignment procedure, and blowing out the dust from the duct and cleaning the windows with lens tissue.

SAFETY ASPECTS

Two areas of the FAM should be considered from the point of view of operator safety: the laser and the high voltage supplies.

As mentioned before the laser beam should never be viewed directly or by reflection on a reflecting surface without protection glasses. The beam can be viewed by reflection from a dull black surface such as felt or flat black optical paint.

There are two potentially accessible high voltage circuits in the FAM: the quadrupole field potentials generated at the high voltage secondaries, and the laser high voltage drive. Caution should be exerted in not touching any of the four terminals at the quadrupole block, nor to separate the small cable connector between the laser power supply and the laser when power is on.

REFERENCES

1. Becklake, M.R., "Asbestos-Related Diseases of the Lung and Other Organs: Their Epidemiology and Implications for Clinical Practice," Am Rev Respir Disease, 114:187. 1976.

2. Bruckman, L., R.A. Rubino, and B. Christine. "Asbestos and Mesothelioma Incidence in Connecticut," Air Pollut Contr Assoc J. 27:121. 1977.

3. Woitowitz, H.J., and H. Valentin. "Arbeitsmedizinische Untersuchungen zur Gesundheits gefährdung durch Asbesthaltige Staube," Staub. 36:112. 1976.

4. Federal Register Sec. 1910.93a added at 36 FR 23207, December 7, 1971, as emergency temporary standard, issued as permanent standard at 37 FR 11318, June 7, 1972, effective July 7, 1972, redesignated Sec. 1910.1001 at 40 FR 23072, May 28, 1975.

5. Edwards, G.H. and J.R. Lynch. The Method Used by the U.S. Public Health Source for Enumeration of Asbestos Dust on Membrane Filters. Ann Occup Hyg. 11:1-6. 1968.

6. Keenan, R.G. and J.R. Lynch. Techniques for the Detection, Identification and Analysis of Fibers. AIHA J. 587. September-October 1970.

7. Addingley, C.G. Asbestos Dust and Its Measurements. Ann Occup Hyg. 9:73-82. 1966.

8. Sampling and Evaluating Airborne Asbestos Dust, Division of Training, NIOSH, U.S. Department of HEW, PHS, Cincinnati, Ohio 45202. April 1974.

9. Davies, R., R. Karuhn, J. Graf, and J. Stockham. The Rapid Counting and Sizing of Fibers in a Mixture Using an IITRI-modified Coulter-Counter, Am Ind Hyg Assoc J. 36:825. 1975.

10. Tolles, W.M., R.A. Sanders, and G.W. Fritz. Dielectric Response of Anisotropic Polarized Particles Observed With Microwaves: A New Method for Characterizing the Properties of Nonspherical Particles in Suspension. Appl Phys J. 45:3777. 1974.

11. Wallach, M.L., and H. Benoit. Light Scattering by Poly-L-Benzyl Glutamate Solutions Subject to an Electric Field. Polymer Sci J. 45:41. 1962.

12. Schwarz, G., M. Seito, and H.P. Schwan. On the Orientation of Nonspherical Particles in an Alternating Electric Field. Chem Phys J. 43:3562. 1965.

13. Jennings, B.R. and H.G. Jerard. Light Scattering Study of Tobacco Mosaic Virus Solutions When Subjected to Electric Fields. Chem Phys J. 44:1291. 1966.

14. Kielich, S. Orientation of Colloid Particles in Laser Optical Fields and Its Effect on Light Scattering of Colloids. J Colloid Interface Sci. 28:214. 1968.

15. Jennings, B.R. and H. Plummer. A Study of Light Scattered by Hectorite Solutions When Subjected to Electric Fields. J Colloid Interface Sci. 27:377. 1968.

16. Wallach, M.L. and H. Benoit. Light Scattering of Polar Chain Molecules Subjected to Electrical Field. J Polym Sci. 4:491. 1966.

17. Stoylov, S.P. and S. Sokerov. Transient Electric Light Scattering. J Colloid Interface Sci. 24:235. 1967.

18. Timbrell, V. Desired Characteristics of Fibers for Biological Experiments. Inst Occup and Environ Health Conference. Fibres for Biological Experiments. Quebec, Canada. October 29, 1973.

19. Timbrell, V. Alignment of Respirable Asbestos Fibres by Magnetic Fields. Ann. Occup Hyg J. 18:299. 1975.

20. Fuchs, N.A. Mechanics of Aerosols. New York, Pergamon Press. 1964.

21. Smythe, W.R. Static and Dynamic Electricity, 2nd Edition. McGraw-Hill, Inc. 1950.

22. Van de Hulst, H.C. Light Scattering by Small Particles. J. Wiley and Sons, Inc. p. 304. 1957.

23. Farone, W.A., M. Kerker and Matijevic. Scattering of Infinite Cylinders at Perpendicular Incidence. In: Electromagnetic Scattering. M. Kerker (ed.). Pergamon Press, Macmillan Company. 1963.

24. Larkin, B.K. and S.W. Churchill. Scattering and Absorption of Electromagnetic Radiation by Infinite Cylinders. J Opt Soc Am. 49:188. 1957.

25. Birkhoff, R.D., et al. Light Scattering From Micron-Size Fibers. Opt Soc Am J. 67:564. 1977.

26. Stoimenova, M.V. Electric Light Scattering by Cylinder-Symmetrical Particles. Colloid Interface Sci J. 53:42. 1975.

27. Lattimer, P. Light Scattering by Ellipsoids. Colloid Interface Sci J. 53:102. 1975.

28. Lundberg, J.L. Light Scattering From Large Fibers at Normal Incidence. Colloid Interface Sci J. 29:565. 1969.

29. Harris, R.L., Jr. and D.A. Fraser. A Model for Deposition of Fibers in the Human Respiratory System. Am Ind Hyg J. 37:73. 1976.

30. Fairchild, C.I., L.W. Ortiz, H.J. Ettinger, and M.I. Tillery. "Aerosol Research and Development Related to Health Hazard Analysis." Los Alamos Scientific Laboratory Report No. LA-6277-PR, March 1976.

31. Anderson, D.P., M.C. Aughlin, H.E. Ayer, and G.A. Carson. Identification of the Quality and Quantity of (Biologically Significant) Cotton Mill Dust. J Occup Med. 15:302. 1973.

32. Lynch, Jr. Air Sampling for Cotton Dust. Transactions, National Conference on Cotton Dust and Health, University of North Carolina, Chapel Hill, 1971.

33. Timbrell, V., A.W. Hyett and J.W. Skidmore. A Simple Dispersion for Generating Dust Clouds From Standard Reference Samples of Asbestos. Ann Occup Hyg J. 11:273. 1968.

34. Spurny, K., C. Boose, and D. Hochrainer. Zur Zerstäubung von Asbestfasern in einem Fliessbett-Aerosolgenerator. Staub. 35:440. 1975.

35. Ortiz, L.W., H.E. Black, and J.R. Coulter. A Modified Fibrous Aerosol Generator. Los Alamos, Scientific Laboratory, Report No. LA-UR-76-1866, 1976.

36. Blair, D.P. and P.H. Sydenham. Phase Sensitive Detection as a Means to Recover Signal Buried in Noise. J Phys E. 8:621. 1975.

37. Moore, R.D. Lock-In Amplifiers for Signals Buried in Noise. Electronics. June 8, 1962.

38. Diamond, J.M. A Double Phase-Sensitive Detector for Bridge Balancing. IEEE Spectrum, p. 62, June 1969.

39. Cole, J.B. and R. M. Duffy. Phase Sensitive Detector and Reference Generator for Use in Third Derivative Locking of the Frequency of a Laser to a Saturated Absorption Feature. J Phys E. 7:1019. 1974.

40. Letzer, S.G. Explore the Lock-In Amplifier. Electron Des. 21:104. October 11, 1974.

41. Lock in the Devil, Feed Him to the Cat, or Take Him for the Last Ride in a Boxcar. Tek Talk, Vol. 6, No. 1, American Dynamics Corporation, Cambridge, Massachusetts.

CONCLUSIONS AND RECOMMENDATIONS

The development of the FAM, described in detail in the foregoing document, represents, in the view of the authors, a significant contribution to the state-of-the-art of aerosol measurement technology and consequently to the methodology available for the detection and assessment of potentially health-injurious airborne fibers.

Although the instrument resulting from this development program is a fully operational and portable device, it should be considered as the prototype it was intended to be, and that both as a result of governmental agency as well as further manufacturer conducted testing, additional operational performance characterization and criteria are expected, and should serve as a basis for further evolution of this promising technique.

Since the presently used method of fibrous-aerosol monitoring is tedious, relatively complex. It is conceivable that this new technique may provide a viable alternative compatible with both short-term as well as a time-averaged monitoring and concurrent recording and/or data transmission. At the least, the FAM will serve as an heretofore unavailable tool for the rapid identification and assessment of sites and conditions associated with excessive fiber concentrations, for the determination of their real-time fluctuations and their correlations with processes and control measures.

Although the FAM development program entailed an intensive laboratory testing activity directed at defining and optimizing the instrument design and operational criteria, the time and funding constraints limited the extent and depth of such activities especially in the characterization of the instrument response for a range of different fibrous aerosols under a variety of concomitant conditions. It is thus recommended that the following areas be pursued in order to more fully establish performance and limitations of the instrument as well as to provide the directions required to extend and improve this technique.

1. Investigation into the effects of, and required measurement discrimination techniques against the presence of large concentrations of potentially interfering particles such as platelets, short (less than 3:1 aspect ratio) elongated particles, and most importantly, irregularly or complex shaped fibers.

2. Determination of the effects of environmental conditions such as humidity, temperature, external electrical interference, shock and vibration, and the long-term exposure to high dust concentrations, in the operation of the FAM.

3. Investigation of design additions and/or modifications in order to both sense and alarm system deviations from operating conditions leading to possible measurement errors as well as to implement corrective measures to compensate for the effect of such conditions.

APPENDIX A

ASSEMBLY DRAWINGS

☆ U.S. Government Printing Office: 1978—757-141/6772, Region No. 5-11

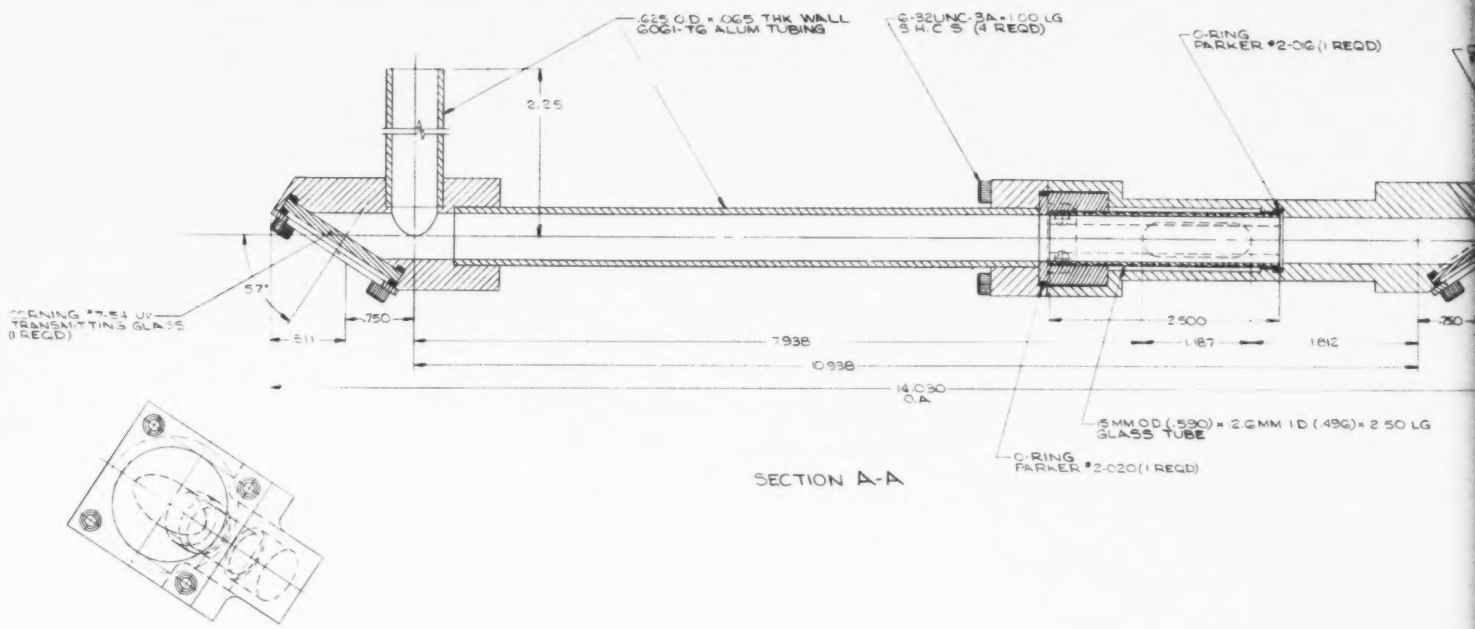

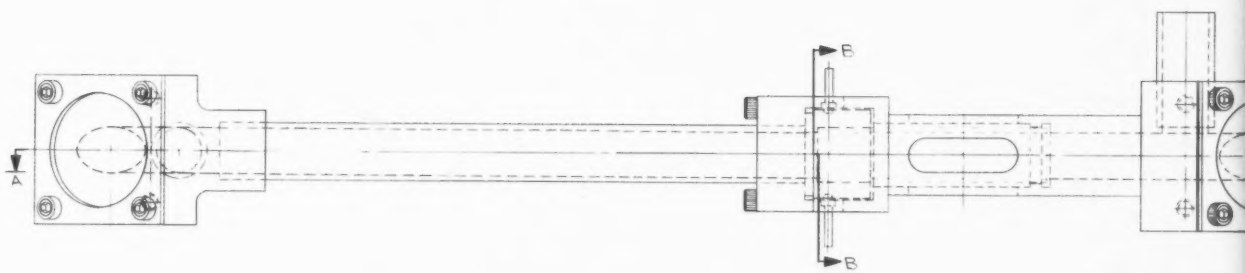

Pages 70 thru 72 blank

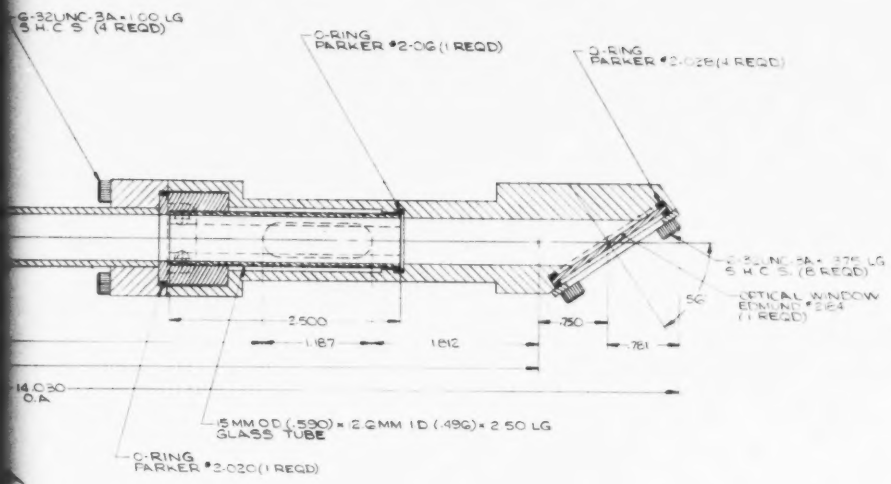

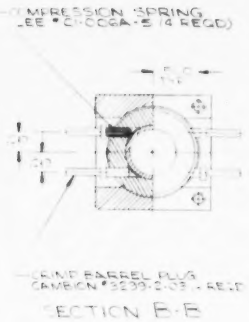

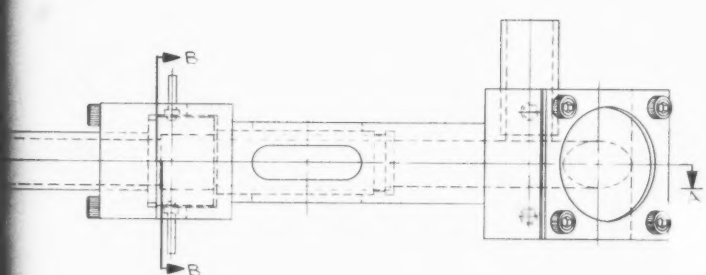

AEROSOL DUCT ASSEMBLY LAYOUT
FIBROUS AEROSOL MONITOR
15 NOV 76

J-375-1019

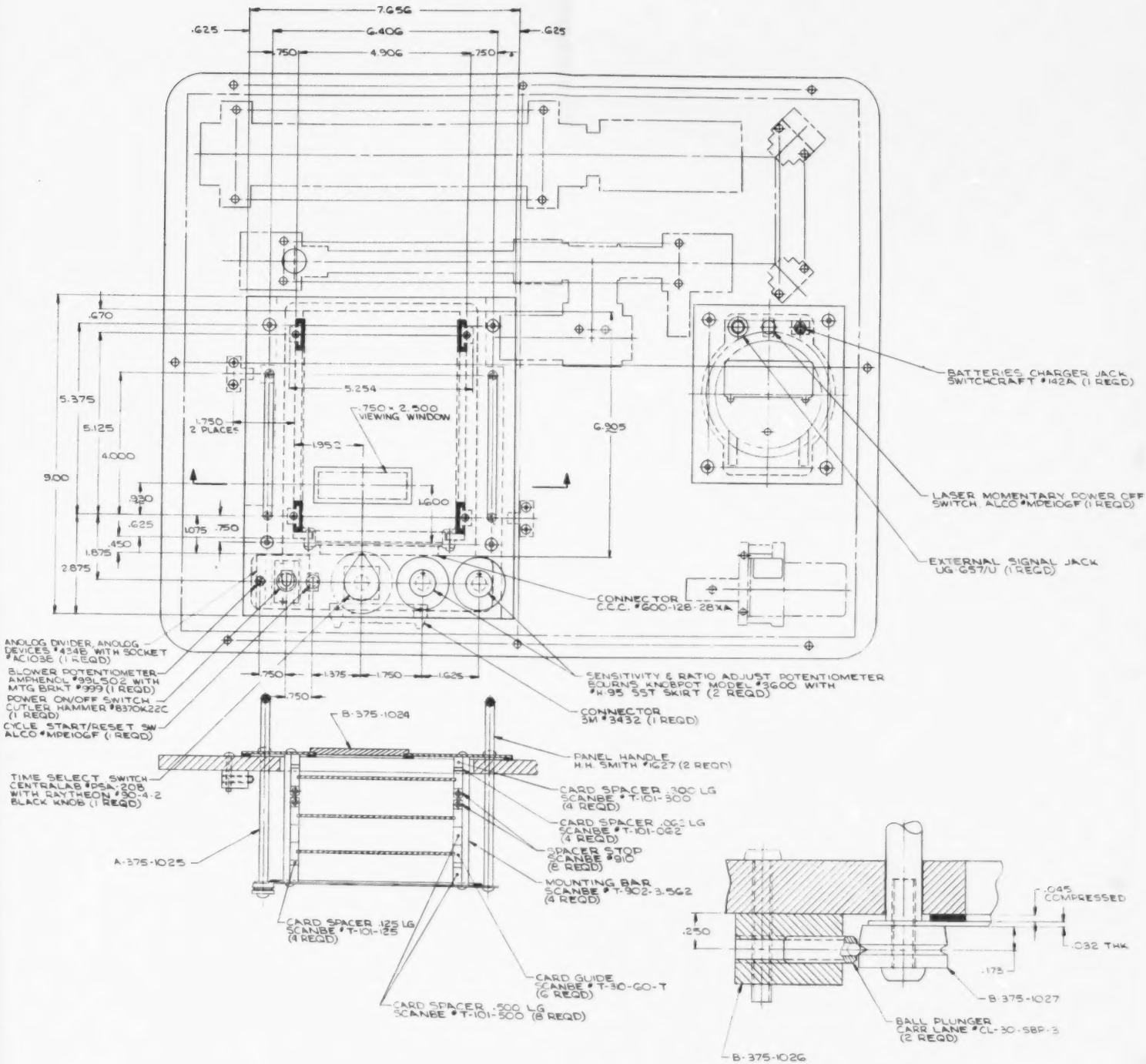

CARD RACK & CONTROL PANELS
LAYOUT

J Jan 30 DEC 76

J-375-1032

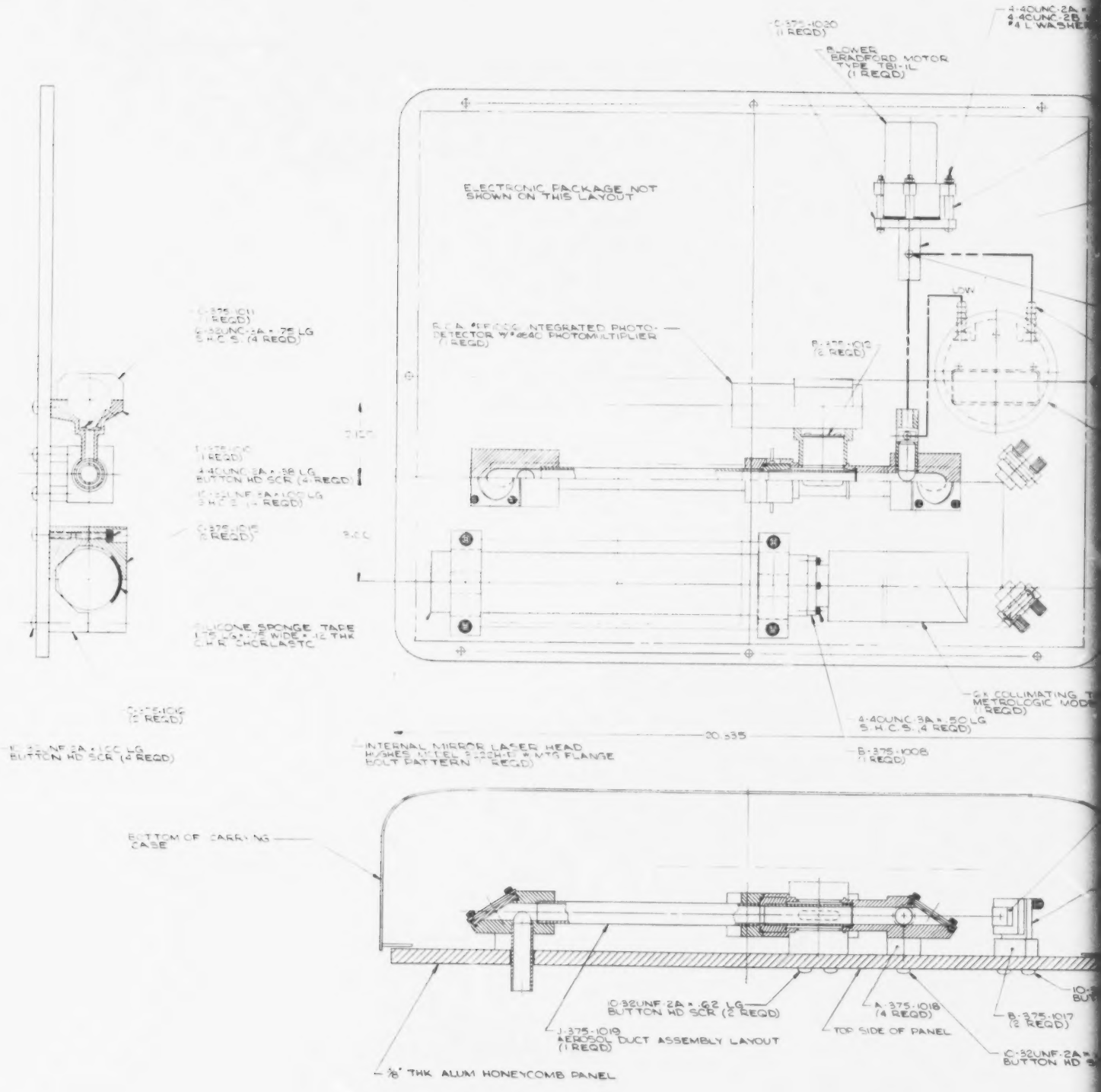

BASE PAN
FIBROU

J-37

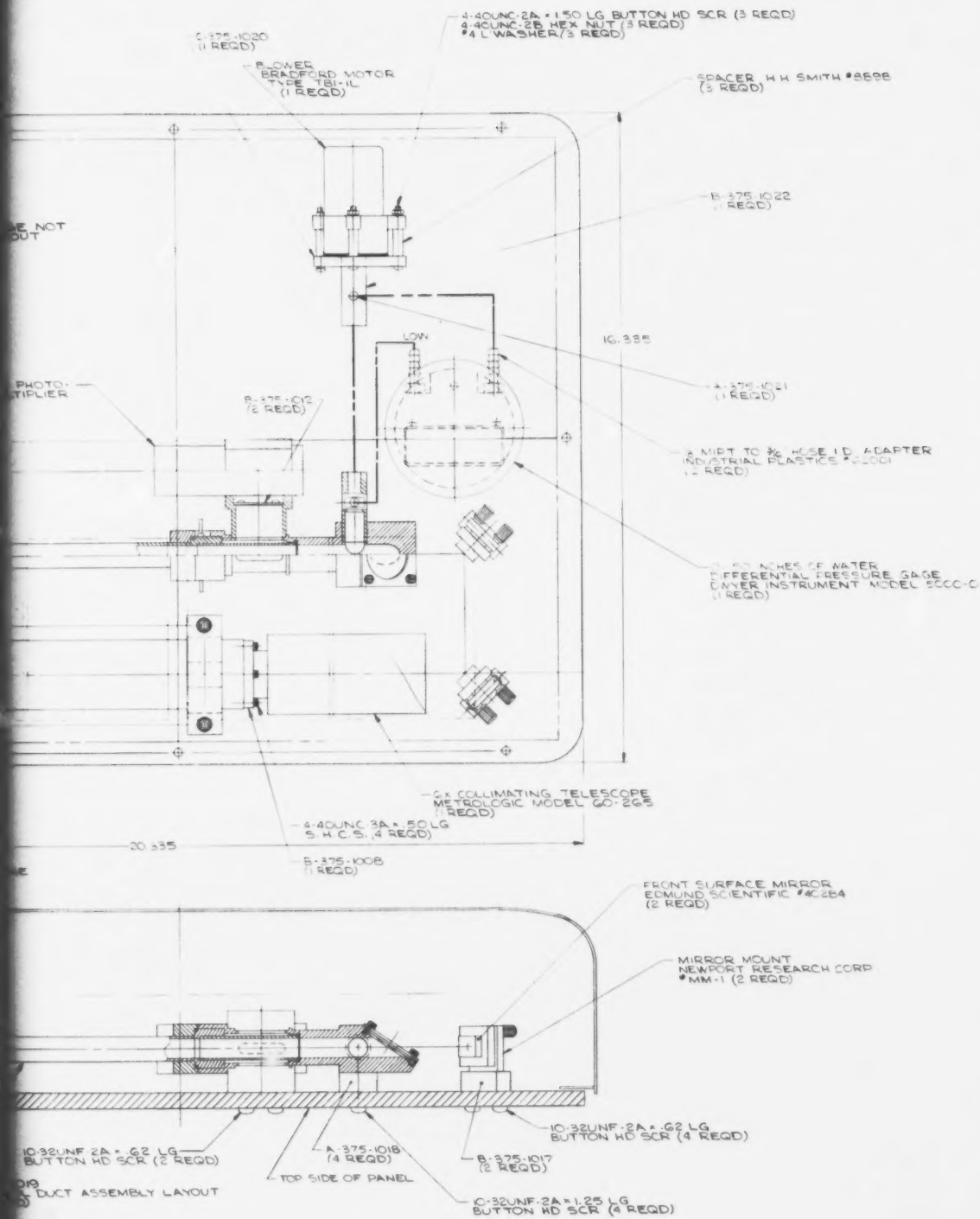

BASE PANEL ASSEMBLY LAYOUT
FIBROUS AEROSOL MONITOR
14 DEC 76

J-375-1023